

Published in final edited form as:

Geochim Cosmochim Acta. 2021 May 15; 301: 158–186. doi:10.1016/j.gca.2021.02.031.

Chromium isotopic insights into the origin of chondrite parent bodies and the early terrestrial volatile depletion

Ke Zhu, Frédéric Moynier^a, Martin Schiller^b, Conel M.O'D. Alexander^c, Jemma Davidson^d, Devin L. Schrader^d, Elishevah van Kooten^{a,b}, Martin Bizzarro^{a,b}

^aUniversite' de Paris, Institut de Physique du Globe de Paris, CNRS UMR 7154, 1 rue Jussieu, Paris 75005, France

^bCentre for Star and Planet Formation, Globe Institute, University of Copenhagen, Øster Voldgade 5-7, Copenhagen DK-1350, Denmark

^cEarth and Planetary Laboratory, Carnegie Institution for Science, 5241 Broad Branch Road, Washington, DC 20015, USA

^dCenter for Meteorite Studies, School of Earth and Space Exploration, Arizona State University, 781 East Terrace Road, Tempe, AZ 85287-6004, USA

Abstract

Chondrites are meteorites from undifferentiated parent bodies that provide fundamental information about early Solar System evolution and planet formation. The element Cr is highly suitable for deciphering both the timing of formation and the origin of planetary building blocks because it records both radiogenic contributions from ⁵³Mn-⁵³Cr decay and variable nucleosynthetic contributions from the stable ⁵⁴Cr nuclide. Here, we report high-precision measurements of the mass-independent Cr isotope compositions ($\epsilon^{53}\text{Cr}$ and $\epsilon^{54}\text{Cr}$) of chondrites (including all carbonaceous chondrites groups) and terrestrial samples using for the first time a multi-collection inductively-coupled-plasma mass-spectrometer to better understand the formation histories and genetic relationships between chondrite parent bodies. With our comprehensive dataset, the order of decreasing $\epsilon^{54}\text{Cr}$ (per ten thousand deviation of the ⁵⁴Cr/⁵²Cr ratio relative to a terrestrial standard) values amongst the carbonaceous chondrites is updated to CI = CH > CR > CM ≈ CV ≈ CO > CK > EC > OC. Chondrites from CO, CV, CR, CM and CB groups show intra-group $\epsilon^{54}\text{Cr}$ heterogeneities that may result from sample heterogeneity and/or heterogeneous accretion of their parent bodies. Resolvable $\epsilon^{54}\text{Cr}$ (with 2SE uncertainty) differences between CV and CK chondrites rule out an origin from a common parent body or reservoir as has previously been suggested. The CM and CO chondrites share common $\epsilon^{54}\text{Cr}$ characteristics, which suggests their parent bodies may have accreted their components in similar proportions. The CB and CH chondrites have low-Mn/Cr ratios and similar $\epsilon^{53}\text{Cr}$ values to the CI chondrites, invalidating them as anchors for a bulk ⁵³Mn-⁵³Cr isochron for carbonaceous chondrites. Bulk Earth has a $\epsilon^{53}\text{Cr}$ value that is lower than the average of chondrites, including enstatite chondrites. This depletion

^{*}Corresponding author. zhu@ipgp.fr (K. Zhu).

Declaration of Competing Interest

The authors declare that they have no known competing financial interests or personal relationships that could have appeared to influence the work reported in this paper.

may constrain the timing of volatile loss from the Earth or its precursors to be within the first million years of Solar System formation and is incompatible with Earth's accretion via any of the known chondrite groups as main contributors, including enstatite chondrites.

Keywords

Chondrites; Genetic relationship; ^{54}Cr systematics; CV-CK, CH-CB and CO-CM clans; CV subgroups; ^{53}Mn - ^{53}Cr chronometry; Condensation history; Volatile depletion; Early Earth; Solar System

1 Introduction

Chondrites are the oldest cosmic sedimentary rocks, the most pristine of which preserve information about the origin of the Solar System (e.g., Krot et al., 2014). Most of the parent bodies of chondrites did not undergo significant melting (though some underwent varying degrees of thermal metamorphism) and thus did not differentiate. Therefore, bulk chondrite samples have chemical compositions that are thought to be representative of the bulk parent body and have been taken as proxies for the composition of bulk differentiated planets such as the Earth (Allègre et al., 1995). Thus, investigating the chemical and isotopic compositions of chondrites is central to better understand the evolution of the Solar System and planet formation. Chondrites also record large chemical and isotopic variations amongst them (Alexander, 2019a,b; Braukmüller et al., 2018; Hellmann et al., 2020; Palme and O'Neill, 2014). In particular, O and Cr isotopes have been key in evaluating genetic links between meteorites and planets (e.g., Clayton and Mayeda, 1999; Qin et al., 2010; Trinquier et al., 2007; Warren, 2011). Although there are several studies utilizing Cr isotopes in this manner, the kinship between different groups of carbonaceous chondrites is still debated. The possible genetic links between the Vigarano-type (CV) and Karoonda-type (CK) chondrites (Dunn and Gross, 2017; Dunn et al., 2016; Greenwood et al., 2010), as well as those of chondrites in Ornans-type (CO) and Mighei-type (CM) groups (e.g., Schrader and Davidson, 2017) and Bencubbin-type (CB) and high-metal (CH) groups are still unresolved (e.g., Krot et al., 2014).

The Cr isotope system may be one of the best suited isotopic systems for studying the timing of chondrite formation and the genetic relationships between meteorite groups (Birck and Allègre, 1988; Trinquier et al., 2007). The short-lived radionuclide ^{53}Mn , with a half-life of 3.7 ± 0.2 Myrs (Holden, 1990), decays to ^{53}Cr and was present in the early Solar System (Lugmair and Shukolyukov, 1998). Therefore, the ^{53}Mn - ^{53}Cr decay system is a useful chronometer to date early Solar System events such as chondrule (precursor) formation (Nyquist et al., 2001; Yamashita et al., 2010; Zhu et al., 2019a; Zhu et al., 2020a), differentiation of planets/asteroids (Lugmair and Shukolyukov, 1998; Trinquier et al., 2008b; Wadhwa et al., 2003; Yamakawa et al., 2010; Zhu et al., 2019b; Zhu et al., 2020b), as well as the aqueous alteration (Fujiya et al., 2012; Fujiya et al., 2013) and possibly the metamorphic processes in chondrite parent bodies (Trinquier et al., 2008b; Göpel et al., 2015). Furthermore, previous Cr isotope measurements have suggested that the various carbonaceous chondrite (CC) groups define a bulk isochron with a slope defining an initial

$^{53}\text{Mn}/^{55}\text{Mn}$ ratio of $(8.5 \pm 1.5) \times 10^{-6}$, which was used to suggest that a volatile fractionation in the solar nebula occurred as early as 4568.6 ± 1.1 Ma (Shukolyukov and Lugmair 2006, Moynier et al. 2007) when the date is anchored to the U isotope corrected age of the D'Orbigny angrite (Amelin, 2008; Brennecka and Wadhwa, 2012; Glavin et al., 2004). This whole-rock ^{53}Mn - ^{53}Cr isochron, reported in Shukolyukov and Lugmair (2006), is primarily controlled by two extreme endmembers representing the Ivuna-type carbonaceous (CI; with the highest $^{55}\text{Mn}/^{52}\text{Cr}$ ratio) and the CB chondrites (with the lowest $^{55}\text{Mn}/^{52}\text{Cr}$ ratio). Based on more recent measurements of the Cr isotopes in CI chondrites (Qin et al., 2010; Trinquier et al., 2008b), Qin et al. (2010) suggested a lower slope of $(5.4 \pm 2.4) \times 10^{-6}$ and a correspondingly younger age of 4566.1 ± 2.4 Ma age for the Mn/Cr fractionation (also anchored to U-corrected D'Orbigny), although this younger age is still consistent within uncertainty with that of Shukolyukov and Lugmair (2006). Finally, the slope of the isochron was later updated to $[(6.2 \pm 1.9) \times 10^{-6}]$ (Göpel et al., 2015). However, all of these isochrons are mostly controlled by the data point for one CB chondrite, Hammadah al Hamra (HaH) 237 (Shukolyukov and Lugmair, 2006) and to date no Cr isotope data for the CH chondrites, which have comparably low Mn/Cr ratios (Lodders et al., 1998), have been reported. Therefore, providing high-precision Cr isotope data for CB and CH chondrites is critical to further evaluate the timing of Mn/Cr fractionation in the early Solar System.

Variable ^{54}Cr nucleosynthetic anomalies, expressed as $\epsilon^{54}\text{Cr}$ (the parts per 10,000 deviation of the mass fractionation corrected $^{54}\text{Cr}/^{52}\text{Cr}$ ratio from a terrestrial standard) have been used as a tracer of potential genetic relationships between Solar System materials (Trinquier et al., 2007) including between Earth and Moon (Mougel et al. 2018). The published $\epsilon^{54}\text{Cr}$ values for several chondrite groups with the mean values following the sequence: CI > CB CR CH CM CV CO CK > EC (Enstatite Chondrites) \approx RC (Rumuruti Chondrites) > OC (Ordinary Chondrites) (Göpel et al., 2015; Mougel et al., 2018; Pedersen et al., 2019; Qin et al., 2010; Shukolyukov and Lugmair, 2006; Trinquier et al., 2007; Van Kooten et al., 2016; Zhu et al., 2021). These isotopic differences between chondrites have been compared to the composition of the Earth's mantle (Mougel et al. 2018) to detect and identify the likely sources of the impact-related extraterrestrial materials included in terrestrial rocks (e.g., Koeberl et al., 2007; Magna et al., 2017; Mougel et al., 2017; Mougel et al., 2019; Schmitz et al., 2016; Trinquier et al., 2006) and to test magma ocean models for asteroids (e.g., Zhu et al., 2019b, 2020b). To date, the most ^{54}Cr -rich phases analyzed in chondrites are 10 s to 100 s of nanometer-size presolar spinel grains that can be concentrated in acid residues (e.g., Podosek et al., 1997; Rotaru et al., 1992) and have been identified by NanoSIMS (Dauphas et al., 2010; Nittler et al., 2018; Qin et al., 2011). These grains probably formed in the ejecta of one or more supernova.

However, although Cr-isotopic homogeneity within each chondrite group is generally assumed, this assertion is only based on a limited number of measurements, often of the same meteorites. In several instances, when two or more meteorites from the same group have been analyzed their $\epsilon^{54}\text{Cr}$ values differ by more than the reported uncertainties of the measurements, including: Renazzo-type carbonaceous (CR) (1.06 ± 0.08 to 1.32 ± 0.11 [2SE] for Northwest Africa [NWA] 7837 and Graves Nunataks [GRA] 06100); CO (0.57 ± 0.11 to 0.87 ± 0.18 , Lance' and Kainsaz); CK (0.33 ± 0.12 to 0.63 ± 0.09 for Elephant Moraine [EET] 92002 and Karoonda) and CV (0.71 ± 0.15 to 1.10 ± 0.08 , for Leoville

and Allende) (Qin et al., 2010; Trinquier et al., 2007; Zhu et al., 2020b). Hence, a more comprehensive Cr isotope dataset is required to better understand the extent of the $\epsilon^{54}\text{Cr}$ variability within and between chondrite groups and to better determine the $\epsilon^{54}\text{Cr}$ sequence for chondrites, especially for the CH and CB chondrites, which lack systematic $\epsilon^{54}\text{Cr}$ studies. Additionally, the CK and CV chondrites share many similar features, including: chondrule sizes and abundances (Weisberg et al., 2006), petrological and chemical compositions (Isa et al., 2014), cosmic-ray exposure ages (Scherer and Schultz, 2000), O-isotope compositions (Greenwood et al., 2010) and Ti isotopic anomalies (Trinquier et al., 2009; Zhang et al., 2012) and are considered a clan (the CV-CK clan). Different models have been proposed for their origins, including the single parent body hypothesis where CV and CK chondrites originate from different depths within the same parent body, with the CK3 to CK6 petrologic types at progressively greater depths (Greenwood et al., 2010). This common origin for CV and CK chondrite groups can be tested using the $\epsilon^{54}\text{Cr}$ systematics. $\epsilon^{54}\text{Cr}$ can also be used to track the relationships between chondrites in CM-CO (e.g., Schrader and Davidson, 2017) and CB-CH clans (e.g., Krot et al., 2014).

The mass-independent Cr isotope compositions of meteorites are traditionally measured by thermal ionization mass spectrometry (TIMS) (Birck and Allègre, 1988; Lugmair and Shukolyukov, 1998; Qin et al., 2010; Shukolyukov and Lugmair, 2006; Trinquier et al., 2007; Trinquier et al., 2008a). However, it appears that there are small residual mass-dependent fractionations that cannot be corrected for, which are evident in the correlation of $\epsilon^{53}\text{Cr}$ and $\epsilon^{54}\text{Cr}$ for multiple measurements of standards with a slope of ~ 2 (Bourdon and Fitoussi, 2020; Qin et al., 2010; Trinquier et al., 2006). It has been suggested that such residual mass-dependent isotopic fractionations could potentially arise from isotopic fractionation between different oxidized Cr gas species during evaporation from the filaments during TIMS analysis (Bourdon and Fitoussi, 2020). This would mimic equilibrium isotope fractionation that occurred as Cr evaporated during the formation of bodies such as the Moon and the asteroid 4 Vesta (Sossi et al., 2018; Zhu et al., 2019c). Moreover, the column chemistry in some previous studies can only reach a Cr yield of $\sim 80\%$ (e.g., Qin et al., 2010; Trinquier et al., 2008a; Trinquier et al., 2008b; Zhu et al., 2019a), and sometimes the yield can be as low as $\sim 60\%$ (Kruijer et al., 2020). However, the equilibrium Cr stable isotope fractionation on the column cannot be fully corrected if the yield is low [e.g., $<70\%$; (Larsen et al., 2016; Qin et al., 2010; Trinquier et al., 2008a)], since the different Cr cuts from the columns show mass-independent fractionation with $\epsilon^{53}\text{Cr}$ ranging from -0.2 to $+0.2$ and $\epsilon^{54}\text{Cr}$ ranging from -0.5 to $+0.4$ (Trinquier et al., 2008a). In order to avoid this problem, we have utilized a high-yield ($\sim 95\%$) four-step column chemistry and employ multiple-collector inductively-coupled-plasma mass-spectrometry (MC-ICP-MS) to measure the mass-independent fractionation of Cr isotopes for a self-consistent comprehensive set of chondrite group compositions, including CI, CB (both CBa and CBb subgroups), CH, CR, CM, CV (including the oxidized, oxA after Allende and oxB after Bali, and reduced, Red after Vigarano, subgroups), CO, CK and high-Fe enstatite (EH) chondrite groups (Pedersen et al., 2019; Qin et al., 2010; Trinquier et al., 2007; Trinquier et al., 2008b; Zhu et al., 2021). This study aims to better constrain the genetic relationship between chondrite parent bodies, chondrite parent body processes (redox, thermal metamorphism and aqueous alteration), the

^{53}Mn - ^{53}Cr “isochron” for CCs and other chondrites, and the radiogenic Cr isotopic deficits between chondrites and Earth.

2 Samples and Methods

2.1 Samples and digestion

The sample suite analyzed in this study includes: one CI1 chondrite (Orgueil), three CB3 chondrites (Miller Range [MIL] 05082, Quebrada Chimborazo [QC] 001 and Hammadah al Hamra [HaH] 237), two CH3 chondrites (Pecora Escarpment [PCA] 91467 and Asuka [A] 881020), two CR chondrites (Grosvenor Mountains [GRO] 95577 [CR1] and Al Rais an anomalous [CR2]), five CM chondrites (Scott Glacier [SCO] 06043 [CM1], Nogoya [CM2], Banten [CM2], Jbilet Winselwan [CM2] and Aguas Zarcas, a new CM2 fall from 2019), three CO3 chondrites (Ornans, MIL 07193 and Dominion Range [DOM] 10104), one CV_{3oxA} chondrite (Allende), three CV_{3oxB} chondrites (Bali, Mokoia, and Kaba), two CV_{3red} chondrites (Leoville and Vigarano), four CK chondrites (Allan Hills [ALH] 85002 [CK4], Karoonda [CK4], Elephant Moraine [EET] 92002 [CK5] and Lewis Cliff [LEW] 87009 [CK6]), and one enstatite chondrite, Sahara 97096 [EH3]. We note that, CB and CH chondrites are highly heterogeneous due to their metal-rich nature (Krot et al., 2014) and that the samples analyzed here (<100 mg) may not represent the bulk parent meteorites. We also selected the United States Geological Survey (USGS) terrestrial rock standard DTS-1 (along with Allende) as a reference material to test the precision and accuracy of the data. Furthermore, the Cr isotope compositions of two widely used artificial standards, NIST 3112a and SCP-Cr (ICP-MS elemental standard for Cr), were measured to test for potential non-mass dependent isotopic fractionation of Cr induced during production of the standards and to calibrate possible offsets between studies using different standards [e.g., NIST 3112a was used by Qin et al. (2010) and Zhu et al. (2019a)]. Among these samples, MIL 05082, Aguas Zarcas, Ornans and Bali were chunks, while the other samples are powders. Based on our recording information, the powder of Jbilet Winselwan, Mokoia, Leoville, Vigarano and Sahara 97096 were from original sample masses of 1.01 g, 1.08 g, 1 g, 0.16 g, and ~0.5 g respectively.

The samples were dissolved following the protocol described in Inglis et al. (2018) using Teflon bombs and an Analab EvapoClean, which has been successfully applied in previous studies (Zhu et al., 2019b, 2020b). The procedure involved heating the samples in concentrated HF and HNO₃ (2:1) at 140 °C for two days, drying down the samples and subsequent dissolution of the solid residues in 6 N HCl (also at 140 °C) for another two days to ensure complete digestion of fluorides, and refractory phases such as chromite and spinel. The combination of Teflon bombs and Analab EvapoClean for chondrite dissolution is simple and convenient, resulting in lower blanks compared to traditional dissolution methods, such as PARR™ bomb dissolution (e.g., Zhu et al., 2019c) and alkaline fusion (e.g., Qin et al., 2010). Before the chemical separation of Cr (see below), ~10% aliquots were preserved for subsequent determination of the $^{55}\text{Mn}/^{52}\text{Cr}$ ratio and major element contents.

2.2 Determination of the $^{55}\text{Mn}/^{52}\text{Cr}$ ratios

High-precision ^{53}Mn - ^{53}Cr chronology requires the accurate determination of the $^{55}\text{Mn}/^{52}\text{Cr}$ ratios, which were measured here on a MC-ICP-MS Neptune Plus, using a method that was similar to those employed in previous studies (Göpel et al., 2015; Trinquier et al., 2008a; Zhu et al., 2019b; Zhu et al., 2020b). We initially prepared three Mn-Cr doped artificial standard solutions gravitationally, with Mn-Cr contents of 10-100 ppb, 50-100 ppb and 100-100 ppb and Mn/Cr ratios of ~ 0.1 , ~ 0.5 and ~ 1.0 . The unpurified sample solutions were diluted to a Cr content of ~ 100 ppb. The intensities for ^{55}Mn and ^{52}Cr on Faraday detectors obtained when analyzing the standard and sample solutions ranged from 0.5 V to 5 V, and 10 cycles of 4 seconds each were measured in each analysis to obtain a target precision for the $^{55}\text{Mn}/^{52}\text{Cr}$ ratios better than 0.1%. After establishing a calibration curve ($R^2 > 0.999$) based on the true and measured $^{55}\text{Mn}/^{52}\text{Cr}$ ratios of the three artificial standards, the $^{55}\text{Mn}/^{52}\text{Cr}$ ratios of the chondrite samples could be calculated. The external precisions for the $^{55}\text{Mn}/^{52}\text{Cr}$ ratios are better than 0.5% (2SD, $N = 6$) as determined from multiple measurements of the USGS standards PCC-1 and DTS-1. The final estimated precision of $< 5\%$ (2σ) was determined from a comparison of the PCC-1 and Allende meteorite results with those in the literature (Moynier et al., 2007; Qin et al., 2010; Shukolyukov and Lugmair, 2006; Trinquier et al., 2008a). The determination of the Mn/Cr ratios on Neptune Plus is faster than the standard-addition method (that requires preparation and analysis of at least four solutions per sample; (e.g., Qin et al., 2010; Zhu et al., 2019a) and more accurate than the Mn and Cr content determination (e.g., Pedersen et al., 2019) by quadrupole ICP-MS (5–10%, 2σ). Additionally, introduction of the low-concentration unpurified samples into the MC-ICP-MS does not result in measurable memory effects.

2.3 Column chemistry

Low Cr yields from column chemistry, where Cr isotopes typically fractionate via equilibrium processes, can result in apparent mass-independent Cr isotope variations resulting from inappropriate mass fractionation corrections (Larsen et al., 2016; Qin et al., 2010; Trinquier et al., 2008a). To avoid this issue, a four-step column chemistry for Cr purification with high yield broadly following previous approaches (Bizzarro et al., 2011; Larsen et al., 2018; Larsen et al., 2016; Pedersen et al., 2019; Schiller et al., 2014; Trinquier et al., 2008a) was employed (Table 1). Only ~ 5 mg of samples were dissolved in 10 M HCl and dried down three times before the following column chemistry step to purify the Cr. First, we used an anion chromatographic purification column to efficiently remove Fe in 6 M HCl. Prior to sample loading on cation exchange columns, we used a Cr pre-treatment procedure involving dissolution in 10 M HCl at > 120 °C to efficiently promote the formation of Cr^{3+} -Cl species, which have a low affinity for the cation exchanger and thus elute early (Larsen et al., 2016; Trinquier et al., 2008a). This was followed by elution of Cr on a 1 ml cation exchange column in 20 ml of 0.5 M HNO_3 to remove the major elements including Mg, Ca, Al, Ni (Bizzarro et al., 2011) and collect all the Cr species (major Cr^0 and minor Cr^{2+} and Cr^{3+}) to reach a $> 99\%$ recovery. The samples were then exposed to 0.5 M HNO_3 + 0.6% H_2O_2 at room temperature for > 1 day to promote the formation of Cr^{3+} (Larsen et al. 2016). However, it is difficult to transform all Cr to Cr^{3+} , so the Cr^0 -bearing material is collected in 0.5 ml of the loading solution and 0.5 ml of 0.5 N HNO_3 elution to increase the recovery to $> 95\%$ in the next column. The third clean-up

column involved Cr purification from Al, Fe, V, Ti (and other high-field-strength elements) and Na, K on a small (0.33 ml) cation exchange column using 0.5 M HNO₃, 1 M HF and 6 M HCl (Larsen et al., 2018). Finally, for the fourth column, 0.7 ml of TODGA resin were used in 8 N HCl to remove the residual Fe, V and Ti (stuck on the column) which have isobaric isotopes with ⁵⁴Cr (⁵⁴Fe) and ⁵⁰Cr (⁵⁰V and ⁵⁰Ti) (Pedersen et al., 2019; Schiller et al., 2014). The full procedure typically reaches a total yield between 95% and 99%, and effectively removes any matrix, especially Fe, V and Ti. Low abundances of matrix elements are important for analyses by MC-ICP-MS as all elements present are ionized (unlike the selective thermal ionization of TIMS) generating potential isobaric interferences and altering the mass fractionation behavior. Artificial standards including NIST 979, NIST 3112a and SCP-Cr (The standard for ICP-MS measurements) were passed through the first column chemistry <5 ng, which is negligible compared to the 10–20 µg of Cr processed through the columns. The final Cr solution was dried in ~100 µl of concentrated HNO₃ three times to transform the acid media and remove residual organics (i.e., those from the cation exchange resin).

2.4 Isotope analysis

The Cr isotopic compositions of all the samples were determined using an MC-ICP-MS Neptune Plus located at the Centre for Star and Planet Formation, Globe Institute, University of Copenhagen. Detailed analytical and data reduction methods are described in Zhu et al. (2021), Schiller et al. (2014) and Pedersen et al. (2019). Each sample was measured by sample-standard bracketing using the NIST SRM 979 Cr standard. Sample solutions with ~0.5 ppm of Cr were introduced to the plasma via an ESI Apex IR resulting in ⁵²Cr signals of 20–40 V at an uptake rate of ~0.06 mL/min. Each sample was measured five times. The ⁵³Cr/⁵²Cr and ⁵⁴Cr/⁵²Cr ratios were normalized to a constant ⁵⁰Cr/⁵²Cr ratios of 0.051859 using an exponential law (Lugmair and Shukolyukov, 1998). All the measured isotopic ratios are expressed relative to NIST SRM 979 in the epsilon notations:

$$\epsilon^x Cr = \left(\frac{\left(\frac{xCr}{^{52}Cr} \right)_{sample}}{\left(\frac{xCr}{^{52}Cr} \right)_{NIST\ SRM\ 979}} - 1 \right) \times 10,000, \quad (1)$$

with x = 53 or 54.

In order to control the influence of the potential isobaric interferences from Fe, V and Ti (⁵⁴Fe to ⁵⁴Cr, ⁵⁰V and ⁵⁰Ti to ⁵⁰Cr) and major alkali elements (Na and K), we also performed doping tests for these elements (the doped samples are the corresponding SCP elemental standards of ICP-MS). The external precision was tested on five Allende, five DTS-1 and two Orgueil from aliquots that were each individually purified from the same digestion. We also provide the ε⁵³Cr data for another Ivuna sample of which ε⁵⁴Cr has been reported in Van Kooten et al. (2016) that described the related analytical methods.

3 Results

The Cr isotope data for doping and external precision tests are reported in Table 2 and combined with literature data from Schiller et al. (2014). In Table 3, we compare the ⁵⁵Mn/

^{52}Cr and Cr isotope data for the same chondrites measured in this and previous studies (Göpel et al., 2015; Jenniskens et al., 2012; Kadlag et al., 2019; Langbroek et al., 2019; Mougél et al., 2018; Moynier et al., 2007; Petit et al., 2011; Qin et al., 2010; Sanborn et al., 2019; Schiller et al., 2014; Trinquier et al., 2007; 2008b; van Kooten et al., 2020, 2016; Williams et al., 2020; Zhu et al., 2020a, 2020b). The averaged group Cr isotope data and $^{55}\text{Mn}/^{52}\text{Cr}$ ratios of all the chondrites are reported in Table 4. We also summarize the Cr isotope data for Rumu-ruti (R) chondrites, Earth, Moon, Mars, Vesta and other achondrite parent bodies in Table 5. Relevant literature O isotope data are shown alongside the new Cr isotope data in Tables 4 and 5 (the samples measured for O and Cr isotope compositions are never from the same aliquots). The Cr isotope data (including literature data) for the terrestrial samples are listed in Table 6. We also re-measured the $^{55}\text{Mn}/^{52}\text{Cr}$ ratios on unprocessed dissolution aliquots for the H chondrites reported in Pedersen et al. (2019) using our MC-ICP-MS approach.

The higher precision Cr isotope data (than those typically obtained by TIMS) for DTS-1 (USGS standards), Allende and as well as the Orgueil meteorites reported here are consistent with most previously reported values (Mougél et al., 2018; Qin et al., 2010; Schiller et al., 2014; Trinquier et al., 2007; Trinquier et al., 2008b; Zhu et al., 2019a; Zhu et al., 2019b; Zhu et al., 2020b), providing confidence in the accuracy of our protocol. Based on multiple individually processed aliquots of Allende (5), DTS-1 (5) and Orgueil digestions (2), we estimate the external reproducibility of our data to be better than 0.04 and 0.07 for $\epsilon^{53}\text{Cr}$ and $\epsilon^{54}\text{Cr}$, respectively (Table 2), which is consistent with the estimates from Schiller et al. (2014). The doping tests show that isobaric interferences do not result in resolvable effects when Fe, V and Ti interferences represent less than ~0.1% (2505 ppm to ^{54}Cr), ~2.5% (1438 ppm to ^{50}Cr) and ~1% (14269 ppm to ^{50}Cr), respectively (Table 2). Finally, Na and K have very limited effects even when their concentrations are sub similar to Cr in the analyzed solutions, and they cause no drift in the Cr mass fractionation.

There are no resolvable mass-independent Cr isotope shifts between chondrite falls and finds from the same group, implying that the mass-independent Cr isotope compositions preserved in the meteorites is robust against limited terrestrial weathering. As such, we conclude that the Cr isotope data reported here is accurate within the reported uncertainties.

The $\epsilon^{54}\text{Cr}$ values of the studied CC groups decrease in the following sequence (mean \pm 2SD): CI (1.56 ± 0.07) > CH (1.50 ± 0.07) CB (1.36 ± 0.30) CR (1.28 ± 0.23) > CM (0.92 ± 0.26) \approx CV (0.89 ± 0.30) \approx CO (0.90 ± 0.43) CK (0.51 ± 0.15) (Figs. 1 and 2). Here, the calculated 2SD uncertainty for grouping CI and CH chondrites are 0.05 and 0.01 respectively (Table 4), which are less than the external uncertainty of 0.07 in this study. Thus, we quote the external reproducibility of 0.07 for the $\epsilon^{54}\text{Cr}$ uncertainty of CI and CH chondrites rather than the calculated 2SD. CC reservoirs have $\epsilon^{54}\text{Cr} + 0.3$ higher than Non-CC reservoirs as terrestrial samples and ECs have $\epsilon^{54}\text{Cr}$ values in the range 0-0.2. Resolved intragroup $\epsilon^{54}\text{Cr}$ variability exists within CB, CM, CV and CO chondrite data, whereas no significant intra-group $\epsilon^{54}\text{Cr}$ variability was found amongst CI, CH, CR and CK chondrite data at the level of our precision. The $\epsilon^{54}\text{Cr}$ values are not correlated with the degree of aqueous alteration (CR2 to CR1, CM2 to CM1) and, at least amongst the CK chondrites, they are also not correlated with the extent of thermal metamorphism (CK4 to

CK6) (Table 3). Furthermore, no systematic correlation between $\epsilon^{53}\text{Cr}$ and $\epsilon^{54}\text{Cr}$ values is observed among the CCs, contradicting the claim of a correlation suggested by Shukolyukov and Lugmair (2006).

The carbonaceous chondrites have decreasing $^{55}\text{Mn}/^{52}\text{Cr}$ ratios in the order: CI > CM > CR > CO > CV = CK > CB = CH (Fig. 3a). Despite these differences, the CCs with the highest and lowest $^{55}\text{Mn}/^{52}\text{Cr}$ ratios, the CI and CB-CH chondrites, respectively, have the highest $\epsilon^{54}\text{Cr}$ values (Fig. 1). More importantly, when considering all CC groups there is no systematic increase in $\epsilon^{53}\text{Cr}$ values with increasing $^{55}\text{Mn}/^{52}\text{Cr}$ ratios, based on the data in this study (Fig. 3a). Most CCs have $\epsilon^{53}\text{Cr}$ values ranging from 0 to 0.2, with an average value of $0.15 (\pm 0.13, 2\text{SD}; \pm 0.02, 2\text{SE}; N = 41)$; excluding the silicate separate of CB chondrites). The $\epsilon^{53}\text{Cr}$ values of CI, CR, CM and CB chondrites tend to be slightly higher compared to CH, CO, CV and CK chondrites, although some CO and CM chondrites exhibit indistinguishable $\epsilon^{53}\text{Cr}$ values. Limited intra-group differences in $\epsilon^{53}\text{Cr}$ values that are not correlated with their respective $^{55}\text{Mn}/^{52}\text{Cr}$ ratios also exist in, for example, the CR, CM and CO groups. The $^{55}\text{Mn}/^{52}\text{Cr}$ and $\epsilon^{53}\text{Cr}$ values for most OCs are correlated (Fig. 3b) and a model 1 regression of *Isoplot R* (Vermeesch, 2018) of these data results in a slope of 0.48 ± 0.20 that corresponds to an initial $^{53}\text{Mn}/^{55}\text{Mn}$ of 5.39 ± 2.23 (MSWD = 2.2, 2SE, N = 23) and an initial $\epsilon^{53}\text{Cr}$ (intercept of y axis) of -0.16 ± 0.05 . All the regressions reported in this paper are calculated in the same way. The Cr data for all the ECs (with literature data) reveals no (positive) correlation between Mn/Cr ratio and $\epsilon^{53}\text{Cr}$ (Fig. 3c).

When combined with literature data (Mougel et al., 2018; Trinquier et al., 2007; Trinquier et al., 2008b), the terrestrial samples show minor Cr isotopic heterogeneity (Fig. 4), with average $\epsilon^{53}\text{Cr} = 0.04 (\pm 0.08, 2\text{SD}; \pm 0.02, 2\text{SE}; N = 15)$ and $\epsilon^{54}\text{Cr} = 0.07 (\pm 0.12, 2\text{SD}; \pm 0.03, 2\text{SE}; N = 15)$. There is no obvious difference between samples with different petrology or chemistry (e.g., the basalt and peridotite). The Cr metal standards NIST SRM 3112a and SCP-Cr have indistinguishable Cr isotope compositions from the NIST SRM 979 standard.

4 Discussion

4.1 Comparison of Cr isotope data for chondrites with literature

CI chondrites are dominated by matrix materials and contain very few chondrules and refractory inclusions (Barrat et al., 2012; Krot et al., 2014), making them more homogenous than other types of chondrites. Hence, CI chondrites are good candidates to compare the Cr isotope data from this study with those in the literature. We have listed all the reported Mn/Cr ratios and Cr isotope data for Orgueil in Table 3. For Orgueil, $\epsilon^{54}\text{Cr}$ values generally fall between 1.50 - 1.60, except for the data reported in Kadlag et al. (2019), which are higher ($\epsilon^{54}\text{Cr} = 1.94 \pm 0.12$). For $\epsilon^{53}\text{Cr}$, some studies (Trinquier et al., 2008a, 2008b; Qin et al., 2010; Schiller et al., 2014) report values of around 0.20, except for those in Kadlag et al. (2019), Moynier et al. (2007) and Shukolyukov and Lugmair (2006), all of which report slightly higher values around 0.40. These elemental and isotope inconsistencies cannot be attributed to the influence from carbonates that have high Mn/Cr ratios and high $\epsilon^{53}\text{Cr}$ values, because the $^{55}\text{Mn}/^{52}\text{Cr}$ ratios of CI chondrites reported in all studies are similar (0.80-0.85). As for $^{55}\text{Mn}/^{52}\text{Cr}$ ratios, the data for Allende (0.51), Orgueil (0.94) and Ivuna

(0.93) in Kadlag et al. (2019) are systematically higher than those reported in this study and other literatures (see Table 3). The cause of the inconsistency between Kadlag et al.(2019) and other recent studies is unknown. Stracke et al.(2012) showed that all the 38 Allende samples have an similar $^{55}\text{Mn}/^{52}\text{Cr}$ values, averaging at 0.41 ± 0.02 (that is consistent with the value from our study, 0.42 ± 0.02), while Kadlag et al. (2019) reported a value of 0.51 ± 0.03 . Since Kadlag et al. (2019) used Parr bombs in their dissolution procedures, it is unlikely that incomplete sample dissolution can account for the data inconsistency.

A similar data inconsistency is also be observed in another CI chondrite, Ivuna. Kadlag et al. (2019) reported a $\epsilon^{54}\text{Cr}$ value (1.79 ± 0.20) for Ivuna, which is higher than that reported in other literature (Schiller et al., 2014; Shukolyukov and Lugmair, 2006; Van Kooten et al.,2016), while Williams et al. (2020) reported a lower $\epsilon^{54}\text{Cr}$ value of 1.30 ± 0.09 . As for $\epsilon^{53}\text{Cr}$ values, Shukolyukov and Lugmair (2006) report a higher $\epsilon^{53}\text{Cr}$ value than that of Schiller et al. (2014) and this study, and the data in Kadlag et al. (2019) has a large error (0.17). Both higher $\epsilon^{53}\text{Cr}$ and $\epsilon^{54}\text{Cr}$ values in Kadlag et al. (2019) might be caused by a residual mass-dependent Cr isotope fractionation using TIMS. However, since the authors do not provide data for terrestrial samples, it is difficult to evaluate this hypothesis. Similarly, Shukolyukov and Lugmair (2006) and Williams et al. (2020) did not report data for terrestrial samples and, as such, the accuracy of their data is difficult to evaluate. The reason for the slightly lower $\epsilon^{54}\text{Cr}$ data in Williams et al. (2020) is also not clear since the authors did not report the $\epsilon^{53}\text{Cr}$ data. Note that a residual massdependent fractionation effect would shift both $\epsilon^{53}\text{Cr}$ and $\epsilon^{54}\text{Cr}$ with a factor of $\sim 1:2$ [see Discussion inSection 4.5, and literature (Bourdon and Fitoussi, 2020; Qin et al.,2010; Shukolyukov and Lugmair, 2006; Trinquier et al.,2006, 2008a)].

Despite some inconsistency between the various studies, we list and consider all published data in Table 3. Averaging the all the data in literature and this study gives: Orgueil: $\epsilon^{53}\text{Cr} = 0.29 \pm 0.07$ and $\epsilon^{54}\text{Cr} = 1.60 \pm 0.10$; Ivuna: $\epsilon^{53}\text{Cr} = 0.28 \pm 0.10$ and $\epsilon^{54}\text{Cr} = 1.56 \pm 0.15$ (the uncertainty reflects the 95% confidence interval, which is also used for other chondrite samples with multiple literature data; Tables 3 and 4).

Allende, which is a large fall (mass of ~ 2 tons), has been the subject of extensive Cr isotopic studies. All the Allende data show relatively homogeneous $\epsilon^{53}\text{Cr}$ values (ranging from 0.04 ± 0.06 to 0.16 ± 0.06) but heterogeneous $\epsilon^{54}\text{Cr}$ values, ranging from 0.86 ± 0.09 to 1.10 ± 0.08 (Trinquier et al., 2007; Zhu et al., 2020b). Since the CVs are the chondrites with the highest abundances of refractory inclusions (CAIs – Ca, Al-rich inclusions and AOAs – amoeboid olivine aggregates), which have extreme $\epsilon^{54}\text{Cr}$ values (Trinquier et al., 2009), and they also have chondrules with variable $\epsilon^{54}\text{Cr}$ values (Olsen et al., 2016), the $\epsilon^{54}\text{Cr}$ variability between Allende measurements likely reflect sample heterogeneity at the scales sampled. The average data for Allende: $\epsilon^{53}\text{Cr} 0.11 \pm 0.02$ and $\epsilon^{54}\text{Cr} = 0.95 \pm 0.07$ is reported in Table 4.

We also compared the Cr isotope data for other chondrites analyzed by various workers (samples are listed in Table 3). In Table 4, we list the averages and the 95% confidence interval uncertainties for the averaged values. Within the uncertainties, most analyses of the same meteorites are consistent. Two exceptions are the $\epsilon^{54}\text{Cr}$ values of Jbilet Winselwan

(CM2) (van Kooten et al., 2020) and the $\epsilon^{53}\text{Cr}$ values of Lance' (CO3) (Moynier et al., 2007; Trinquier et al., 2008b). The small-degree of $\epsilon^{54}\text{Cr}$ heterogeneity (0.82 ± 0.04 – 1.01 ± 0.12) in Jbilet Winselwan could also result from sample heterogeneity, given that CM chondrites also contain abundant refractory inclusions (Krot et al., 2014), and their chondrules possess variable $\epsilon^{54}\text{Cr}$ values (van Kooten et al., 2020). Note that the $\epsilon^{53}\text{Cr}$ of Lance, -0.04 ± 0.07 in Trinquier et al. (2008b), is lower than that of most other CO chondrites and even those of all other measured chondrites, and its $\epsilon^{54}\text{Cr}$ value is also lower than all the other CO chondrites. Because the mass of the Lance' aliquot analyzed by Trinquier et al. (2008b) is only 9 mg, it is possible that it is not representative of the bulk parent meteorite. As such, we have not included the $\epsilon^{53}\text{Cr}$ and $\epsilon^{54}\text{Cr}$ values for Lance' in Table 4 and do not consider it in further discussion.

It is also noteworthy to discuss the Cr isotope variation in CB chondrites. The three CB chondrites measured in this study (with different subgroups, i.e., CB, CBa and CBb), MIL 05082, QC 001 and HaH 237 (mostly silicate), have homogeneous $\epsilon^{54}\text{Cr}$ values (1.46 ± 0.08 ; 2SD, $N = 3$), which is inconsistent with those of other previously reported CB chondrites HaH 237 (0.87 ± 0.19) (Shukolyukov and Lugmair, 2006) and Bencubbin (bulk, average of silicate and metal; 1.12 ± 0.03) (Trinquier et al., 2007). Here, since the metal and silicate parts for Bencubbin (Trinquier et al., 2007) and Gujba (Yamashita et al., 2010) have consistent $\epsilon^{54}\text{Cr}$ values, we averaged the $\epsilon^{54}\text{Cr}$ values of their different components to represent their bulk $\epsilon^{54}\text{Cr}$ compositions. The bulk $\epsilon^{54}\text{Cr}$ values of HaH 237 and Bencubbin are different from the average $\epsilon^{54}\text{Cr}$ value of the Gujba components, 1.29 ± 0.07 , (Yamashita et al., 2010), but overlap within uncertainty with the $\epsilon^{54}\text{Cr}$ value (1.07 ± 0.27) of the metal spherules from Gujba (Trinquier et al., 2008b). We do not interpret this $\epsilon^{54}\text{Cr}$ inconsistency as inter-laboratory biases because the Cr isotope data for terrestrial samples from the different studies (including different instruments within the same laboratory) are all consistent within error (Qin et al., 2010; Trinquier et al., 2007, 2008b; Zhu et al., 2019a, 2020a, 2020b). Instead, it is likely that there is some $\epsilon^{54}\text{Cr}$ variability between CB chondrite samples.

The $\epsilon^{54}\text{Cr}$ data for the CO chondrites analyzed in this study (Table 4), ranging from 0.80 ± 0.06 to 1.22 ± 0.04 , are higher than for Fe'lix (0.63 ± 0.09) and Lance' (0.57 ± 0.11) reported in Trinquier et al. (2007), but similar to that of Kainsaz (0.87 ± 0.18) reported in Qin et al. (2010) (Table 4).

4.2 Updated $\epsilon^{54}\text{Cr}$ sequence and intra-group $\epsilon^{54}\text{Cr}$ heterogeneity of carbonaceous chondrites

Chondrites typically have low cosmic ray exposure ages (CREA, less than 100 Ma) and relatively low Fe/Cr ratios (Eugster, 2003; Weber et al., 2001), which limits the potential cosmogenic effects on their Cr isotope compositions. Even amongst Angrites with Fe/Cr ratios of up to 600 and CREA up to 60 Ma (Eugster, 2003; Zhu et al., 2019b) and mesosiderites with CREA up to 300 Ma (Eugster, 2003; Trinquier et al., 2007), their $\epsilon^{54}\text{Cr}$ values remain relatively homogeneous and show no correlation with CREA. As for the Fe-rich CB chondrites, the metal and silicate parts of Bencubbin have the same $\epsilon^{54}\text{Cr}$ values, again showing that cosmogenic effects are not detectable in them with current

measurement precisions. Therefore, $\epsilon^{54}\text{Cr}$ signatures are a robust tool for tracing general genetic relationships of chondrite parent bodies.

In Table 4, combining these new measurements with literature data (Göpel et al., 2015; Qin et al., 2010; Trinquier et al., 2007; van Kooten et al., 2020; Zhu et al., 2021) results in an updated $\epsilon^{54}\text{Cr}$ sequence: CI < CH < CB < CR > CM \approx CV \approx CO < CK > EC \approx RC > OC (Fig. 1). We note that the CB and CH chondrite samples in this study may not represent a bulk sample due to the sample heterogeneity. However, the CB chondrite components (e.g., chondrules, silicates and metal) have homogeneous $\epsilon^{54}\text{Cr}$ values (Trinquier et al., 2007; Yamashita et al., 2010), perhaps owing to their formation mechanism by impact (Krot et al., 2005). Thus, the $\epsilon^{54}\text{Cr}$ data reported here for CB chondrites can be used to estimate the bulk value of the parent meteorite. We note that the $\epsilon^{54}\text{Cr}$ systematics in CH chondrite components needs to be studied in the future. This updated sequence provides new insights into confirming the classification of meteorites linked to recognized meteorite groups and determining potential genetic affinities between ungrouped chondrites and recognized meteorite groups. However, since our new data show an overlap in the $\epsilon^{54}\text{Cr}$ values of CM, CV and CO chondrites, the applicability of the $\epsilon^{54}\text{Cr}$ systematics as a tracer in carbonaceous meteorites is weaker than originally suggested (e.g., Trinquier et al., 2007). Aguas Zarcas fell on April 23, 2019 in Costa Rica and was classified as a CM2 chondrite (the Meteorite Bulletin #108). This chondrite is of significant interest as it contains abundant prebiotic compounds similar to other CM chondrites (Glavin et al., 2020). The Cr isotopic data for Aguas Zarcas from this study, with $\epsilon^{53}\text{Cr} = 0.15 \pm 0.03$; $\epsilon^{54}\text{Cr} = 0.86 \pm 0.03$, is consistent with the $\epsilon^{54}\text{Cr}$ variation range of CM chondrites ($\epsilon^{54}\text{Cr} = 0.92 \pm 0.24$, 2SD).

The $\epsilon^{54}\text{Cr}$ and D^{17}O values of CCs were previously reported to be correlated (Trinquier et al., 2007). However, this correlation was based on a limited data set and the Cr and O isotope data were often not from the same chondrites (see Fig. 2; Trinquier et al., 2007). Our new data (same chondrites, but not the same sample aliquots for Cr and O isotope measurements) show that this correlation ($R^2 = 0.58$) is not as robust as previously observed. Nonetheless, our data confirm the Cr isotopic difference between the CCs and most other (e.g., OCs, RCs and ECs) meteorites (Trinquier et al., 2007; Warren, 2011), which is also observed for Ti (Trinquier et al., 2009; Zhang et al., 2012), Ca (Dauphas et al., 2014; Schiller et al., 2018), Ni (Steele et al., 2012); Mo (Budde et al., 2016; Spitzer et al., 2020; Yokoyama et al., 2019), and Ru (Fischer-Gödde et al., 2015; Fischer-Gödde and Kleine, 2017).

An important new observation shown by our extended database is the intragroup $\epsilon^{54}\text{Cr}$ variability among the CB, CM, CO, and CV chondrites (Figs. 1 and 2). This is consistent with reported intra-group heterogeneities for bulk Ti isotope anomalies (expressed as $\epsilon^{50}\text{Ti}$) amongst the CM, CV and CO chondrites (Trinquier et al., 2009; Zhang et al., 2012). One of the best examples of this is the Allende CV chondrite whose published $\epsilon^{54}\text{Cr}$ values range from 0.86 ± 0.09 to 1.10 ± 0.08 (Qin et al., 2010; Trinquier et al., 2007; Zhu et al., 2020b). Similarly, the three CB chondrites studied here: MIL 05082 (CB), QC 001 (CBa), and HaH 237 (CBb) have indistinguishable $\epsilon^{54}\text{Cr}$ values with a mean of 1.46 ± 0.08 (2SD, $N = 3$). This is in contrast to the previously reported data for CBs that are significantly different in their absolute values and more variable, e.g., 1.29 ± 0.07 (2SD; average value

of the chondrules and metal in Gujba) for Gujba, and 1.12 ± 0.03 (2SD) for Bencubbin (Trinquier et al., 2007; Yamashita et al., 2010), but marginally overlaps with the $\epsilon^{54}\text{Cr}$ data (1.07 ± 0.27) for one metal chondrule in Gujba (Trinquier et al., 2008a, 2008b). We also find that some CH and CB chondrites have comparable $\epsilon^{54}\text{Cr}$ compositions to CIs, which until now were considered the most ^{54}Cr -enriched chondrites in bulk. The intragroup $\epsilon^{54}\text{Cr}$ heterogeneity of the CB, CM, CO, and CV chondrites likely result from sample heterogeneity at the scale of most measured samples that is also reflected by intragroup (e.g., CM, CB, CV, or CR) or even intra-chondrite (e.g., Jbilet Winselwan, Paris, and NWA 8157) O isotope variability (see Fig. 2 and Table 4). However, the O isotope compositions (D^{17}O) can also change as a result of aqueous alteration (Schrader et al., 2014; Schrader et al., 2011) and terrestrial weathering (Alexander et al., 2018). Mineral and acid leachates exhibit very large Cr isotope variability (Göpelet et al., 2015; Podosek et al., 1997; Qin et al., 2010; Rotaru et al., 1992; Schiller et al., 2014; Trinquier et al., 2007; Wang et al., 2011). The CM, CO, and CV chondrites also contain large fractions of CAIs and AOAs (5 vol.%, 13 vol.%, and 10 vol.%, respectively; Krot et al., 2014; Weisberg et al., 2006) that have high $\epsilon^{54}\text{Cr}$ values of up to ~ 6 (Larsen et al., 2011; Trinquier et al., 2009) but relatively low Cr contents. Although chondrules recorded heterogeneous $\epsilon^{54}\text{Cr}$ values (e.g., Bollard et al., 2019; Olsen et al., 2016; Qin et al., 2011; Schneider et al., 2020; van Kooten et al., 2020; Zhu et al., 2019a, 2020a), it is unlikely that they are the cause the $\epsilon^{54}\text{Cr}$ heterogeneity between bulk chondrites from same groups because OCs, ECs and CK chondrites, which have chondrules showing clear $\epsilon^{54}\text{Cr}$ heterogeneity (Bollard et al., 2019; Williams et al., 2020; Zhu et al., 2020a), have homogeneous $\epsilon^{54}\text{Cr}$ values. Schneider et al. (2020) report that various matrix material in Allende have a fairly narrow range of $\epsilon^{54}\text{Cr}$ values (1.06 ± 0.22 ; 2SD, $N = 3$) and, as such, a variable chondrule/matrix ratio could also contribute to the variability of the $\epsilon^{54}\text{Cr}$ values between CCs groups. It should be noted that the OCs and ECs have high abundances (60-80%) of chondrules (Krot et al., 2014), which is consistent with the $\epsilon^{54}\text{Cr}$ homogeneity in OCs and ECs, since the chondrule/matrix-ratio effect should be less in OCs and ECs than that in CCs. Alternatively, the limited $\epsilon^{54}\text{Cr}$ heterogeneity within the OCs, ECs, RCs and CKs (maybe also CR; Bunch et al., 2008) could also be the result of metamorphic homogenization. Since they are not as metamorphosed, the apparent intragroup $\epsilon^{54}\text{Cr}$ heterogeneity of CM, CO and CV chondrites (CV chondrules possess the most variable $\epsilon^{54}\text{Cr}$ values, ranging from -0.79 to 2.01; Olsen et al., 2016) may be mainly due to the relatively small sample size and non-representative sampling. This is consistent with the observation that 0.6-1 g of Allende may not be enough to be representative for the average bulk composition (Stracke et al., 2012).

It is unlikely that metamorphism can explain the $\epsilon^{54}\text{Cr}$ homogeneity in type-3 OCs, ECs and RCs. Also, the effect of sample size and CAI-AOA abundance cannot explain the $\epsilon^{54}\text{Cr}$ heterogeneity amongst the CR and CB chondrites, because they have low combined CAI and AOA contents (less than 0.5 vol.%; Scott and Krot, 2005) and chondrules with almost homogeneous $\epsilon^{54}\text{Cr}$ values (Olsen et al., 2016; Yamashita et al., 2010). Alternatively, it is possible that the intra-group $\epsilon^{54}\text{Cr}$ heterogeneity in CCs (mainly CV, CO, CM, CB and CR groups) reflects $\epsilon^{54}\text{Cr}$ heterogeneity in their parent bodies at scales that are larger than represented by the meteorites. This is also consistent with the variable major element compositions, abundances of their components (e.g., CAIs) and O isotope compositions

(Fig. 2) in different chondrite samples from the same group (Ebel et al., 2016; Hezel et al., 2008). Note that $\epsilon^{54}\text{Cr}$ heterogeneities have also been found within achondrite groups, e.g., ureilites (Zhu et al., 2020b), so it is also possible that some parent bodies (e.g., CV, CO, CM and CB) are isotopically heterogeneous.

4.3 Constraints on parent body processes and possible genetic relationships (CV-CK, CM-CO and CB-CH clans) inferred from $\epsilon^{54}\text{Cr}$ systematics

The lack of correlated intragroup $\epsilon^{54}\text{Cr}$ values with the degree of aqueous alteration (i.e., CR2 to CR1, CM2 to CM1) or thermal metamorphism (i.e., CK4 to CK6) also suggests that parent body processes did not redistribute the Cr at the scales we have sampled (e.g., Qin et al., 2010; Trinquier et al., 2007). This is also consistent with previous studies, indicating that petrologic types 3 to 6 in both the OCs and ECs have the same $\epsilon^{54}\text{Cr}$ values within their uncertainties (Mougel et al., 2018; Qin et al., 2010; Trinquier et al., 2007).

Our new $\epsilon^{54}\text{Cr}$ data also allow us to evaluate if the CV sub-groups originate from an isotopically homogeneous, common parent body. The three CV subgroups primarily differed from one another in their redox states: oxidized CV_{oxA}, CV_{oxB} and the reduced CV_{red}. These CV subgroups may either originate from two or three different parent bodies (Gattacceca et al., 2020; Greenwood et al., 2010) or, alternatively, from different regions of a single parent body (Greenwood et al., 2010). Based on the presence of CV_{oxB}-type clasts in the CV_{red} chondrite Vigarano (Krot et al., 2000) and clasts of CV_{oxB} and CV_{oxA} lithologies in the oxidized CV Mokoia (Krot et al., 1998), the origins of these subgroups from separate parent bodies already appears unlikely. Our data show that meteorites from these three subgroups have indistinguishable $\epsilon^{54}\text{Cr}$ signatures (e.g., CV_{oxA}: Allende with $\epsilon^{54}\text{Cr}$ of 0.95 ± 0.06 ; CV_{oxB}: Bali, Mokoia and Kaba with $\epsilon^{54}\text{Cr}$ of 0.70 ± 0.07 to 1.10 ± 0.06 ; CV_{red}: Leoville and Vigarano with $\epsilon^{54}\text{Cr}$ of 0.76 ± 0.10 and 0.85 ± 0.02 , respectively, Table 3), consistent with their origin from a single parent body and that internal redox variations did not alter their bulk $\epsilon^{54}\text{Cr}$ compositions. This is inconsistent with the systematically different O isotope compositions between oxidized and reduced CV chondrites (Clayton and Mayeda, 1999; Gattacceca et al., 2020). Combined with their distinct chondrule sizes and matrix abundances, Gattacceca et al. (2020) argued there are multiple CV chondrite parent bodies. Since CV_{ox} and CV_{red} chondrites have similar $\epsilon^{54}\text{Cr}$ values, and O isotopes are sensitive to aqueous alteration (e.g., Farquhar et al., 1998), an alternative explanation for the relationship between CV_{ox} and CV_{red} sub-groups is the regional heterogeneity in water/rock ratio within a single parent body.

Based on chemical and petrological similarities and similar O-isotope compositions, the CV and CK chondrites have been grouped into the CV-CK clan and are considered by some to have originated from the same parent body (Greenwood et al., 2010). Nonetheless, the CV and CK chondrites are still considered different chondrite groups based on relative differences in the abundances of their bulk refractory lithophile elements and CAIs, and the presence of coarse-grained igneous rims around chondrules in CV chondrites that are almost absent in the CK chondrites (Kallemeyn et al., 1991). To reconcile the similar O-isotope compositions but the small chemical and textural differences between CV and CK chondrites, it has been proposed that the CK chondrites (which exist as petrologic

types 3 to 6) formed deeper in the same parent body as the CV chondrites (which are exclusively low petrologic type 3 s) (Greenwood et al., 2010; Wasson et al., 2013). This scenario is consistent with thermal modeling (Elkins-Tanton et al., 2011). Our high-precision Cr isotope data reveal that the CK chondrites have similar $\epsilon^{54}\text{Cr}$ values to one another, 0.51 ± 0.15 (2SD), ± 0.08 (2SE, N = 4), but are significantly lower than those of the CV chondrites ($\epsilon^{54}\text{Cr}=0.89\pm 0.30$ [2SD], ± 0.12 [2SE, N=6]). This confirms the first resolvable difference between the $\epsilon^{54}\text{Cr}$ values of one CV and one CK chondrite reported in Trinquier et al. (2007). Given the lack of evidence that secondary parent body processes, including aqueous alteration, thermal metamorphism and redox processes can significantly affect $\epsilon^{54}\text{Cr}$ at the scale we sampled, the different $\epsilon^{54}\text{Cr}$ values for CV and CK chondrites imply that they did not originate from the same parent reservoir. This is also supported by the different chemical composition of magnetites in CV and CK chondrites, suggesting that they experienced different metamorphic histories (Dunn et al., 2016).

Similarly, CM and CO chondrites, which are in the CM-CO clan (Weisberg et al., 2006), share mineralogical and geochemical similarities, including anhydrous mineral compositions and bulk elemental and O-isotope compositions (Clayton and Mayeda, 1999; Greenwood and Franchi, 2004; Kallemeyn and Wasson, 1981; Weisberg et al., 2006), which is consistent with their similar $\epsilon^{54}\text{Cr}$ compositions. As such, our Cr isotope data further supports the idea that the CM and CO chondrite precursors formed from similar materials. However, they cannot derive from the same parent body, because (1) their mean chondrule sizes are resolvably different and their chondrules (mainly type II chondrules) have different petrologic characteristics (Schrader and Davidson, 2017), (2) the CM chondrite parent body likely formed approximately 1 million years after the CO chondrite parent body (Sugiura and Fujiya, 2014).

The CB and CH chondrites form the same clan (Krot et al., 2014) and both of them have high $\epsilon^{54}\text{Cr}$ values (>1.1). However, the CBs have heterogeneous $\epsilon^{54}\text{Cr}$ values, while those of the CHs are homogeneous. Furthermore, the CB (MIL05082) and CH (PCA 91467 and A-881020) chondrites have similar $^{55}\text{Mn}/^{52}\text{Cr}$ ratios but different $\epsilon^{53}\text{Cr}$ values, which is likely caused by their different initial $\epsilon^{53}\text{Cr}$ values and/or formation times. This suggests different origins for the CB and CH chondrites, which is consistent with their different $\epsilon^{54}\text{Cr}$ features, i.e. the $\epsilon^{54}\text{Cr}$ heterogeneity and homogeneity in the CB and CH chondrite parent bodies, respectively. However, the numbers of CB and CH samples that have been measured are still small and measurements of more CBs and CHs are needed to confirm our conclusions.

4.4 ^{53}Mn - ^{53}Cr systematics of bulk chondrites

The previously postulated CC ^{53}Mn - ^{53}Cr isochron was mostly controlled by a single CB chondrite, HaH 237 with low $^{55}\text{Mn}/^{52}\text{Cr}$ of 0.08 and $\epsilon^{53}\text{Cr}$ of -0.15 ± 0.09 , and two CI chondrites, Orgueil and Ivuna, with high $^{55}\text{Mn}/^{52}\text{Cr}$ of ~ 0.8 and $\epsilon^{53}\text{Cr}$ of ~ 0.4 (see the grey points and line in Fig. 3a) (Moynier et al., 2007; Shukolyukov and Lugmair, 2006). Subsequently, Trinquier et al. (2008b) and Qin et al. (2010) determined that using an updated $\epsilon^{53}\text{Cr}$ values for CI chondrites of ~ 0.2 , the age of the “isochron”, decreases from 4568.6 ± 1.1 Ma to 4566.1 ± 2.4 Ma (the two ages are still consistent within uncertainty).

At that time, no CH chondrites had been studied. Here we show that our sample of HaH 237 (mostly silicates) has a similar $^{55}\text{Mn}/^{52}\text{Cr}$ (0.09) to that reported by Shukolyukov and Lugmair (2006) but a higher $\epsilon^{53}\text{Cr}$ value (0.05 ± 0.03). The two CB chondrites MIL 05082 and QC 001 have $^{55}\text{Mn}/^{52}\text{Cr}$ ratios of 0.37-0.47 and $\epsilon^{53}\text{Cr}$ values of 0.20 ± 0.01 (2SD, $N = 2$) that are indistinguishable from CI chondrites (0.21 ± 0.04 ; 2SD, $N = 2$). Moreover, the CH chondrites in this study with the lowest Mn/Cr ratios have $\epsilon^{53}\text{Cr}$ values of 0.12 ± 0.03 that are too high to be consistent with the postulated isochron. Although our new values suggest that the CH and CB chondrites are not consistent with a common CC isochron, a potential caveat with this observation is the difficulty in obtaining samples that are representative of the bulk meteorites. We note that while there is a broad correlation between bulk CC $^{55}\text{Mn}/^{52}\text{Cr}$ ratios and $\epsilon^{53}\text{Cr}$ values, these data do not form a single well-defined ^{53}Mn - ^{53}Cr isochron even when the CH and CB chondrites are excluded (Fig. 3a).

There are several likely reasons for the lack of a single, well-defined ^{53}Mn - ^{53}Cr isochron among the CCs. Firstly, unlike other CCs, the CH and CB chondrites probably formed via impacts that postdated the formation of other CCs (Krot et al., 2005; Yamashita et al., 2010), and the impact, e.g., ~5 Ma after CAIs (Krot et al., 2005), may potentially and secondarily modify the Mn/Cr ratios (Krot and Nagashima, 2017; Weisberg et al., 2001). Thus, there is no *a priori* reason why they should form a common ^{53}Mn - ^{53}Cr isochron with the other CCs. Secondly, all eight CC groups have distinct photochemical and/or nucleosynthetic isotope anomalies (Clayton and Mayeda, 1999; Schiller et al., 2018; Trinquier et al., 2009; Zhang et al., 2012) reflecting variability in the makeup of their precursors and/or their formation environments within the proto-planetary disk. Finally, chondrites are complex assemblages of CAIs, AOAs, chondrules and matrix (Alexander, 2019a) that formed at different times and under varying conditions (Connelly et al., 2012). The chondritic components (i.e., chondrules, matrix, metals, CAIs and AOAs) do not all have the same ages and/or source regions (initial $\epsilon^{53}\text{Cr}$ values). For example, although CAIs and some chondrules did form at the same time (see the internal isochron ages; Connelly et al., 2012; Bollard et al., 2017), these objects have distinct nucleosynthetic anomalies (Cr and Ti: Trinquier, et al. 2009; Olsen et al., 2016; Gerber et al., 2017; Schneider et al., 2020; Williams et al., 2020; Zhu et al., 2019a; Zhu et al., 2020a), and, as such, must have formed in distinct reservoirs. Some CO and CM chondrites have similar $^{55}\text{Mn}/^{52}\text{Cr}$ ratios but distinct $\epsilon^{53}\text{Cr}$ values, which indicates that on average their components experienced Mn/Cr fractionation at different times and/or conditions. Their different radiogenic Cr isotopic compositions also supports CM and CO chondrites originating from different parent bodies (e.g., Schrader and Davidson, 2017). The matrix also has a distinct origin based on its variable nucleosynthetic isotope signatures (Cr, Ti, Mo and W; Budde et al., 2016; Schneider et al., 2020). This has also been discussed in Zhu et al. (2020a) and Alexander (2019a). Overall, the ^{53}Mn - ^{53}Cr correlation for most chondrites is almost certainly a multiple-component mixing trend. However, this mixing for CC ^{53}Mn - ^{53}Cr correlation line is not limited to only chondrule-matrix (e.g., Anders, 1964), because CK chondrites with high abundance of matrix (~75%; Krot et al., 2014) also have low Mn/Cr ratios compared to most of other CC groups (Fig. 3a). Considering that the half-life of ^{53}Mn is comparable to the accretion ages of chondrites, it is perhaps unsurprising that a general trend resembling a ^{53}Mn - ^{53}Cr isochron between chondrite groups exists.

Such a correlation is stronger for the OCs than the CCs (Fig. 3b). The calculated initial $^{53}\text{Mn}/^{55}\text{Mn}$ ratio for this OC trend is $(5.39 \pm 2.23) \times 10^{-6}$. When anchored to D'Orbigny with the absolute age (U isotope-corrected) of 4563.37 ± 0.25 Ma and an initial $^{53}\text{Mn}/^{55}\text{Mn}$ of $(3.24 \pm 0.04) \times 10^{-6}$ (Amelin, 2008; Brennecka and Wadhwa, 2012; Glavin et al., 2004), this is equivalent to an age of 4566.1 ± 2.3 Ma. However, this apparent isochron for the OCs may not have chronological significance, even considering that the $\epsilon^{54}\text{Cr}$ and $\Delta^{17}\text{O}$ values suggest a common origin for this group, because the correlation line can also result from mixing of different proportions of chondritic components. Compared to the CCs, the OCs have fewer refractory inclusions, more chondrules, less matrix and variable amount of metal ($\text{H} > \text{L} > \text{LL}$). The mixing end-members are thus chondrules, matrix and metal, and the metal should play a more important role in the mixing. This is because the metal-rich H chondrites possess lower $^{55}\text{Mn}/^{52}\text{Cr}$ ratios and lower $\epsilon^{53}\text{Cr}$ values, compared to metal-poor LL chondrites, with intermediate L chondrites (Fig. 3b) (Krot et al., 2014). Fig. 3c shows there is no resolved positive slope in a ^{53}Mn - ^{53}Cr correlation diagram. Note that ECs are composed of chondrules, metals (Krot et al., 2014) and many Mn- or Cr-rich sulfide minerals (e.g., Piani et al., 2016; Zhu et al., 2020a). Metals are poor in both Mn and Cr, and silicate usually possess more Mn than Cr (Piani et al., 2016) such that, their sulfide minerals have large variability for Mn and Cr contents (e.g., Cr-rich troilite and Mn-rich niningerite; Piani et al., 2016), so their complicated ^{53}Mn - ^{53}Cr mixing budgets may obscure any ^{53}Mn - ^{53}Cr correlation.

When comparing the ^{53}Mn - ^{53}Cr data for all chondrite groups (Fig. 4), there is no well-defined ^{53}Mn - ^{53}Cr isochron. Actually, nearly half of the data points do not fit on the regression line. However, all the different groups of chondrites here define a positive trend between $\epsilon^{53}\text{Cr}$ values and $^{55}\text{Mn}/^{52}\text{Cr}$ ratios. For example, the CV, CK, CO, and CH chondrites mostly possess low $^{55}\text{Mn}/^{52}\text{Cr}$ ratios ($< \sim 0.5$) and $\epsilon^{53}\text{Cr}$ values, $< \sim 0.12$, while the CI, CM, CR (except one in van Kooten et al., 2020), and OCs mostly have high $^{55}\text{Mn}/^{52}\text{Cr}$ ratios ($> \sim 0.5$) and $\epsilon^{53}\text{Cr}$ values, $> \sim 0.12$. These variations may be caused by a multiple-endmember mixing of the different chondritic components (chondrules, matrix, CAIs and AOAs) that on average experienced Mn/Cr fractionations at different times, reflecting a general relationship between $^{55}\text{Mn}/^{52}\text{Cr}$ ratios and $\epsilon^{53}\text{Cr}$ values. Regressing all the ^{53}Mn - ^{53}Cr data for all the chondrites [by model 3 (maximum likelihood regression with overdispersion) due to the $\text{MSWD} \gg 1$, *Isoplot R* (Vermeesch, 2018)], the slope is 0.285 ± 0.078 with initial $\epsilon^{53}\text{Cr} = 0.00 \pm 0.05$ ($\text{MSWD} = 11$, $N = 85$). This slope corresponds to a $^{53}\text{Mn}/^{55}\text{Mn} = (3.23 \pm 0.89) \times 10^{-6}$ and an absolute age of 4563.4 ± 1.5 Ma, when anchored to the U isotope-corrected D'Orbigny angrite. However, this ^{53}Mn - ^{53}Cr correlation line likely represent a mixing line that does not have any chronological significance.

Trinquier et al. (2008a, 2008b) included a number of chondrites (OC, EC, CI, CV, and CO groups) and planets/asteroids (including Earth, Mars and Vesta) on the same ^{53}Mn - ^{53}Cr diagram with a slope of $(6.53 \pm 1.93) \times 10^{-6}$ and an absolute age of 4567.3 ± 1.9 Ma. They interpreted this age as the last isotopic equilibration of Mn and Cr in the protoplanetary disk. The chondrites and planets had distinct origins and formation times, which violates the primary assumption of an isochron that all components formed at the same time from the same reservoir. Thus, any ^{53}Mn - ^{53}Cr correlation is a mixing line that does not have any chronological significance either. Here, it should also be mentioned that the

age from a ^{53}Mn - ^{53}Cr “isochron” established by acid leachates in chondrites (Göpel et al., 2015; Trinquier et al., 2008b) are also questionable and mostly reflect mixing lines. This is because (1) The chondritic components, e.g., CAIs, chondrules, matrix, metal and carbonates, have different origins and formed at different periods, which has been discussed in the previous section. For example, only five leachates, out of 15, of Orgueil CI chondrite fall on a single ^{53}Mn - ^{53}Cr correlation line (Trinquier et al., 2008b). This possibly reflects the fact that CI chondrites experienced secondary aqueous alteration and thereby forming resulting in the formation of younger carbonates (that would be dissolved by the weak acid, e.g., acetic acid, in the first step of leaching) with high Mn/Cr ratios (e.g., Fujiya et al., 2012; Fujiya et al., 2013), although CI chondrites are mostly composed of matrix material, and contain few CAIs and chondrules (Krot et al., 2014). The chondrites that have abundant CAIs, AOAs and chondrules, e.g., CV and CO chondrites, have a more complex ^{53}Mn - ^{53}Cr mixing process; (2) Mn is rich in the easily dissolved minerals with high Mn/Cr ratios, e.g., carbonates, while Cr is rich in the refractory phases with low Mn/Cr ratios, e.g., chromites, so the acid leachates potentially represent the components of high-Mn/Cr and low-Mn/Cr reservoirs, which mostly reflects mixing lines that do not have chronological meaning. This is consistent with the anomalous $^{53}\text{Mn}/^{55}\text{Mn}$ [$(13.64 \pm 0.01) \times 10^{-6}$; corresponding to 4571.1 ± 0.9 Ma that is older than CAIs] and initial $\epsilon^{53}\text{Cr}$ values (-0.61 ± 0.05) obtained from a ^{53}Mn - ^{53}Cr correlation line of acid leachates of the Paris chondrite (Göpel et al., 2015).

4.5 The $\epsilon^{53}\text{Cr}$ deficit between chondrites and Earth suggests early volatile depletion of Earth precursors

The 15 terrestrial samples (including basalts, peridotites and chromites; including both MC-ICP-MS data in this study and TIMS literature data; see Table 6) measured relative to NIST SRM 979 and corrected for mass bias using the kinetic fractionation law exhibit $\epsilon^{53}\text{Cr}$ and $\epsilon^{54}\text{Cr}$ values that are slightly positive with 0.04 ± 0.08 (2SD); 0.02 (2SE) and 0.09 ± 0.12 (2SD); 0.03 (2SE), respectively (Fig. 5). The slightly positive $\epsilon^{53}\text{Cr}$ and $\epsilon^{54}\text{Cr}$ for terrestrial samples has been linked to an isotope fractionation behavior that differs from the kinetic fractionation of atomic Cr in the mass spectrometers that was induced during the preparation of the NIST 979 standard (Schiller et al., 2014). Similar mass-independent isotopic difference between terrestrial rocks and purified metal standards (i.e., NIST 3112a and SCP-Cr) have also been observed for other elements like Ni (Steele et al., 2011), Sr (Moynier et al., 2012), Ti (Zhang et al., 2012), and Mo (Budde et al., 2019). As such, the reported average $\epsilon^{54}\text{Cr}$ values of terrestrial samples are currently the best estimate of the bulk terrestrial mass-independent Cr isotope composition. The residual variability in terrestrial rock analyses highlights Cr isotope fractionation in nature and/or during Cr purification and TIMS analysis that do not follow the kinetic law for Cr, perhaps because they involved molecular species (e.g., CrO_2) (see Fig. 6).

This is supported by the fact that theoretical calculations predict that inappropriate mass fractionation correction should result in apparent mass-independent effects on $\epsilon^{53}\text{Cr}$ and $\epsilon^{54}\text{Cr}$. Chromium evaporates not only as Cr^+ , but multiple oxidized species such as CrO , CrO_2 and CrO_3 may also be present during heating and evaporation during TIMS ionization. Based on masses and abundances stated in Table 7a, we firstly calculated the

fractionation factors, $\beta^{53}\text{Cr}$ and $\beta^{54}\text{Cr}$ for different Cr species following Young and Galy (2004). In detail, the factors for equilibrium and kinetic fractionation laws are calculated from Eqs. (9) and (12), respectively, in Young and Galy (2004). Then, we determined the $^{53}\text{Cr}/^{52}\text{Cr}$ and $^{54}\text{Cr}/^{52}\text{Cr}$ ratios for a given $^{50}\text{Cr}/^{52}\text{Cr}$ fractionation and fractionating species. We subsequently derive the relative deviations resulting from non-kinetic and/or non-atomic Cr isotope fractionation from the predicted Cr isotope ratios resulting from the typically applied mass bias correction based on kinetic laws and atomic Cr for these isotope ratios (^{53}Cr and ^{54}Cr) (Table 7b). Irrespective of the fractionating Cr species, the apparent anomalies in the $^{53}\text{Cr}/^{52}\text{Cr}$ and $^{54}\text{Cr}/^{52}\text{Cr}$ ratios (^{53}Cr and ^{54}Cr) co-vary with a factor of ~ 2.6 , which also mimics the slope (2.6) of the reported $\epsilon^{53}\text{Cr}$ and $\epsilon^{54}\text{Cr}$ values of multiple measurements for NIST 3112abyTriton TIMS (Qin et al., 2010). This ratio is also broadly consistent with the $\epsilon^{53}\text{Cr}$ vs. $\epsilon^{54}\text{Cr}$ values amongst the terrestrial samples (Fig. 5) that exhibit a slope of ~ 2 considering that the magnitude of isotopic variability is typically on the order of the analytical uncertainty. However, small variations in $\epsilon^{53}\text{Cr}$ and $\epsilon^{54}\text{Cr}$ in natural terrestrial samples may not solely be due to instrumental effects but may be the product of natural equilibrium Cr stable isotope fractionation, i.e., the Cr stable isotope fractionation during magmatic process where fractionation occurs based on exchange of Cr^{2+} and Cr^{3+} .

The average $\epsilon^{53}\text{Cr}$ value, 0.04 ± 0.02 (2SE, N = 15), of all terrestrial samples provides the current best estimate for the Cr isotopic composition of the BSE. It should be noted that Cr is more siderophile than Mn during core formation (Mann et al., 2009), resulting in elevated $^{55}\text{Mn}/^{52}\text{Cr}$ ratios in the BSE compared to the core. If the Earth core formation process occurred early (e.g., chiller et al., 2020), i.e. before ^{53}Mn extinction, the higher Mn/Cr ratio of BSE compared to the core would theoretically produce higher $\epsilon^{53}\text{Cr}$ in the BSE relative to the core. Based on a mass balance calculation:

$$\text{Bulk Earth} = \text{Bulk Silicate Earth} + \text{Core} \quad (2)$$

the $\epsilon^{53}\text{Cr}$ values of the bulk earth (BE) should be similar to (if Earth core formed after ^{53}Mn extinction) or slightly lower than (if Earth core formed before ^{53}Mn extinction) that of BSE.

Since the $\epsilon^{53}\text{Cr}$ value of the BSE is lower than that of chondrites, the $\epsilon^{53}\text{Cr}$ of BE must also be lower. The $\epsilon^{53}\text{Cr}$ value of BSE of 0.04 ± 0.02 (2SE, N = 15) is systematically lower than the average $\epsilon^{53}\text{Cr}$ value of all the chondrites, $\epsilon^{53}\text{Cr} = 0.16 \pm 0.01$ [2SE, N = 88; see Fig. 5; (Trinquier et al., 2008b)]. We tested the significance of the $\epsilon^{53}\text{Cr}$ isotopic difference between chondrites (N = 88) and Earth (N = 15) by running an unpaired student t-test using Prism 8, which returned a P-value < 0.0001 confirming the statistical difference between the two groups (statistical difference is considered for P-value < 0.05). The BE also has a lower $\epsilon^{53}\text{Cr}$ value compared to ECs ($\epsilon^{53}\text{Cr} = 0.15 \pm 0.03$; 2SE, N = 12; average $^{55}\text{Mn}/^{52}\text{Cr} = 0.71$) that have been used as analogues for the isotopic composition of Earth's precursors via protracted stochastic collisional accretion given their otherwise close nucleosynthetic match to the BSE (Javoy et al., 2010), and CI chondrites ($\epsilon^{53}\text{Cr} = 0.22 \pm 0.02$; 2SE, N = 2; average $^{55}\text{Mn}/^{52}\text{Cr} = 0.82$) that represent the bulk chemical composition of Solar System (Alle`gre et al., 1995; Krot et al., 2014). This $\epsilon^{53}\text{Cr}$ deficit between chondrites and Earth has been already observed in previous studies (Qin et al., 2010; Trinquier et al., 2008b), and

interpreted as representing early Mn/Cr volatile fractionation (Palme and O'Neill, 2014). Here, we combined all the chondrite data in this study and literature to better constrain the early volatile depletion of the Earth.

Variability in the initial abundance of the $^{53}\text{Mn}/^{55}\text{Mn}$ within the early Solar System is unlikely to cause this discrepancy given that the CCs and non-CCs have similar $\epsilon^{53}\text{Cr}$ values (Trinquier et al., 2008b), and the relative ^{53}Mn - ^{53}Cr ages of some achondrites (e.g., Sanborn et al., 2019; Zhu et al., 2019b) and chondrules (Bollard et al., 2015; Krot et al., 2005; Yamashita et al., 2010; Zhu et al., 2019a, 2020a) are consistent with absolute Pb-Pb chronometry. As such, the cause for this $\epsilon^{53}\text{Cr}$ difference between the BSE and chondrites must be due to Mn/Cr fractionation prior to the extinction of ^{53}Mn (half-life of 3.7 Myrs). The $^{55}\text{Mn}/^{52}\text{Cr}$ ratio of the BE is difficult to estimate precisely. However, it has been estimated that the $^{55}\text{Mn}/^{52}\text{Cr}$ ratio of the bulk Earth is between 0.22 and 0.54 (Palme and O'Neill, 2014; Sun, 1982; Wang et al., 2018; Wänke Dreibus, 1988), which is lower than those of the CIs (~0.82) and ECs (~0.71). The ECs have similar isotopic compositions as Earth for multiple elements (Clayton et al., 1984; Javoy et al., 2010; Mougél et al., 2018; Piani et al., 2020; Trinquier et al., 2007; Zhu et al., 2020a), and CIs are proxies for the chemical composition of the bulk Solar System (Alle`gre et al., 1995). The lower $^{55}\text{Mn}/^{52}\text{Cr}$ ratio for BE is likely caused by preferential evaporative loss of Mn relative to Cr either prior to or during Earth's accretion. We can estimate the timing of the volatile depletion by calculating a minimum age of volatile loss. To that end, we calculate the evolving $\epsilon^{53}\text{Cr}$ signature of BE using the initial $\epsilon^{53}\text{Cr}$ and $^{53}\text{Mn}/^{55}\text{Mn}$ abundance of the Solar System (Trinquier et al., 2008a, 2008b) assuming a single stage Mn-loss that reduced the initial Mn/Cr ratio of the accreting Earth to its current value between 0.22 and 0.54. From this estimate, it becomes apparent that lowering of the Mn/Cr ratio of the Earth must have occurred within 0-3 Myr after CAI formation. This age is also consistent with another volatile-sensitive chronometer, the ^{87}Rb - ^{87}Sr system that indicates that the planetary volatile depletion events happened very early, i.e., in the first few Myrs after CAIs (Gray et al., 1973; Hans et al., 2013; Moynier et al., 2012).

It should be noted that decreasing the Mn/Cr ratios from chondrites to Earth would be consistent with stronger volatilization of Mn than Cr (Sossi et al., 2019). In fact, this age of proto-Earth volatilization is consistent with the ^{53}Mn - ^{53}Cr age of chondrule precursors (Zhu et al., 2019a, 2020a) that have been considered as potential candidates for the building blocks of terrestrial planets by the mechanism of pebble accretion (Johansen et al., 2015; Schiller et al., 2018; Schiller et al., 2020). In particular, pebble accretion inevitably results in hot planetary atmospheres and proto-planets (Popovas et al., 2018) providing a natural mechanism of early volatile loss of the accreting Earth at early times (Mahan et al., 2018; Rubin et al., 1988). Therefore, our data suggest that the terrestrial volatile depletion more likely occurred during the formation of Earth precursors as opposed to later volatile loss during planetary evolution. In particular, evaporation under planetary conditions is predicted to occur under more oxidizing conditions (Visscher and Fegley Jr, 2013), which could make Cr more volatile than Mn (Sossi et al., 2019). This would result in an increase of the Mn/Cr ratio and subsequently the $\epsilon^{53}\text{Cr}$ of the devolatilized planet compared to chondrites, which is the opposite of what is observed.

5 Conclusion

This study reports a new comprehensive mass-independent Cr isotope dataset of numerous chondrite types as well as Earth, using improved methods for high-yield purification method and high-precision Cr isotope measurements by MC-ICP-MS. The main conclusion of our work can be summarized as follows:

1. Our $\epsilon^{54}\text{Cr}$ chondrite data complement earlier work, and provide an updated decrease of $\epsilon^{54}\text{Cr}$ as follows: $\text{CI} \sim \text{CH} \sim \text{CB} \sim \text{CR} > \text{CM} \approx \text{CV} \approx \text{CO} > \text{CK} > \text{E-C} > \text{OC}$. Our data also show that CB, CM, CV, CR and CO chondrites have intra-group $\epsilon^{54}\text{Cr}$ heterogeneities that are likely caused by unrepresentative sampling or heterogeneous accretion of chondrite parent bodies.
2. The distinct $\epsilon^{54}\text{Cr}$ for CV and CK chondrites suggest that they do not come from the same parent body, whereas the indistinguishable $\epsilon^{54}\text{Cr}$ values of CM and CO chondrites suggest their parent bodies share common precursor materials and, thus, may have formed under similar conditions. Moreover, heterogeneous $\epsilon^{54}\text{Cr}$ values for CB chondrites compared to the homogeneous $\epsilon^{54}\text{Cr}$ values for CH chondrites suggests they may have different origins.
3. The low-Mn/Cr CH and CB chondrites have indistinguishable $\epsilon^{53}\text{Cr}$ values from those of high-Mn/Cr CI chondrites and, as such, these data are inconsistent with the proposed bulk CC ^{53}Mn - ^{53}Cr isochron. The broad correlation between Mn/Cr ratios and $\epsilon^{53}\text{Cr}$ values in chondrites may simply reflect a mixing line between high- and low-Mn/Cr ratio reservoirs.
4. When compared to the NIST SRM 979 Cr standard, bulk (silicate) Earth is characterized by $\epsilon^{53}\text{Cr}$ and $\epsilon^{54}\text{Cr}$ values of 0.04 ± 0.02 and 0.09 ± 0.03 (2SE), respectively. The correlated and slightly positive values reflect non-kinetic isotopic fractionation of the NIST SRM 979 Cr standard and some terrestrial samples. The lower $\epsilon^{53}\text{Cr}$ of bulk silicate Earth compared to chondrites requires early volatile loss of Earth's precursor materials. Based on the half-life of ^{53}Mn (3.7 Ma), this volatile loss likely occurred within 3 Myr of Solar System formation.

Acknowledgements

We deeply appreciate Thorsten Kleine for efficient editorial handling and detailed and constructive comments from Herbert Palme, Anne Trinquier and one anonymous reviewer, which greatly improved this manuscript. F. M. acknowledges funding from the European Research Council under the H2020 framework program/ERC grant agreement (#637503-PRISTINE) and financial support of the UnivEarthS Labex program at Sorbonne Paris Cite' (#ANR-10-LABX-0023 and #ANR-11-IDEX-0005-02), and the ANR through a chaire d'excellence Sorbonne Paris Cite'. Parts of this work were supported by IGP multidisciplinary program PARI, and by Paris-IdF region SESAME (#12015908). M. B. acknowledges funding from the Carlsberg Foundation (CF18-1105), the Danish National Research Foundation (DNRF97) and the European Research Council (ERC Advanced Grant Agreement, #833275-DEEPTIME). M. S. acknowledges funding from the Villum Fonden (#00025333). E.v.K. acknowledges funding from the European Union's Horizon 2020 research and innovation programme under the Marie Skłodowska-Curie Grant Agreement No786081. We also appreciate the Arizona State University Center for Meteorite Studies for providing some of the samples used in this study. US Antarctic meteorite samples are recovered by the Antarctic Search for Meteorites (ANSMET) program which has been funded by NSF and NASA, and characterized and curated by the Department of Mineral Sciences of the Smithsonian Institution and Astromaterials Acquisition and Curation Office at NASA.

Johnson Space Center. Timothy Mock is appreciated for providing the Cr isotope standard of NIST SRM 3112a. K. Z. thanks the China Scholarship Council (CSC) and IPGP for a PhD fellowship (#201706340161) and the Aide à la MOBILITE INTERNATIONALE des doctorants de l'IPGP (2019), respectively.

References

- Alexander CMOD. Quantitative models for the elemental and isotopic fractionations in chondrites: The carbonaceous chondrites. *Geochim Cosmochim Acta*. 2019a; 254 :277–309.
- Alexander CMOD. Quantitative models for the elemental and isotopic fractionations in the non-carbonaceous chondrites. *Geochim Cosmochim Acta*. 2019b; 254 :246–276.
- Alexander CMOD, Greenwood RC, Bowden R, Gibson JM, Howard KT, Franchi IA. A multi-technique search for the most primitive CO chondrites. *Geochim Cosmochim Acta*. 2018; 221 :406–420.
- Allègre CJ, Poirier J-P, Humler E, Hofmann AW. The chemical composition of the Earth. *Earth Planet Sci Lett*. 1995; 134 :515–526.
- Amelin Y. U-Pb ages of angrites. *Geochim Cosmochim Acta*. 2008; 72 :221–232.
- Anders E. Origin, age, and composition of meteorites. *Space Sci Rev*. 1964; 3 :583–714.
- Barrat JA, Zanda B, Moynier F, Bollinger C, Liorzou C, Bayon G. Geochemistry of CI chondrites: Major and trace elements, and Cu and Zn Isotopes. *Geochim Cosmochim Acta*. 2012; 83 :79–92.
- Birck J-L, Allègre CJ. Manganese—chromium isotopes systematics and the development of the early Solar System. *Nature*. 1988; 331 :579–584.
- Bischoff A, Vogel N, Roszjar J. The Rumuruti chondrite group. *Geochemistry*. 2011; 71 :101–133.
- Bizzarro M, Paton C, Larsen K, Schiller M, Trinquier A, Ulfbeck D. High-precision Mg-isotope measurements of terrestrial and extraterrestrial material by HR-MC-ICPMS—implications for the relative and absolute Mg-isotope composition of the bulk silicate Earth. *J Anal At Spectrom*. 2011; 26 :565–577.
- Bollard J, Connelly JN, Bizzarro M. Pb-Pb dating of individual chondrules from the CBA chondrite Gajba: Assessment of the impact plume formation model. *Meteorit Planet Sci*. 2015; 50 :1197–1216. [PubMed: 27429545]
- Bollard J, Connelly JN, Whitehouse MJ, Pringle EA, Bonal L, Jørgensen JK, Nordlund A, Moynier F, Bizzarro M. Early formation of planetary building blocks inferred from Pb isotopic ages of chondrules. *Sci Adv*. 2017; 3 e1700407 [PubMed: 28808680]
- Bollard J, Kawasaki N, Sakamoto N, Olsen M, Itoh S, Larsen K, Wielandt D, Schiller M, Connelly JN, Yurimoto H, Bizzarro M. Combined U-corrected Pb-Pb dating and ^{26}Al - ^{26}Mg systematics of individual chondrules – Evidence for a reduced initial abundance of ^{26}Al amongst inner Solar System chondrules. *Geochim Cosmochim Acta*. 2019; 260 :62–83.
- Bourdon B, Fitoussi C. Isotope fractionation during condensation and evaporation during planet formation processes. *ACS Earth Space Chem*. 2020; 4 :1408–1423.
- Braukmüller N, Wombacher F, Hezel DC, Escoube R, Münker C. The chemical composition of carbonaceous chondrites: Implications for volatile element depletion, complementarity and alteration. *Geochim Cosmochim Acta*. 2018; 239 :17–48.
- Brennecka GA, Wadhwa M. Uranium isotope compositions of the basaltic angrite meteorites and the chronological implications for the early Solar System. *Proc Natl Acad Sci*. 2012; 109 :9299–9303. [PubMed: 22647606]
- Budde G, Burkhardt C, Brennecka GA, Fischer-Gödde M, Kruijer TS, Kleine T. Molybdenum isotope evidence for the origin of chondrules and a distinct genetic heritage of carbonaceous and non-carbonaceous meteorites. *Earth Planet Sci Lett*. 2016; 454 :293–303.
- Budde G, Burkhardt C, Kleine T. Molybdenum isotopic evidence for the late accretion of outer Solar System material to Earth. *Nat Astron*. 2019; 1
- Bunch TE, Irving AJ, Wittke JH, Rumble D, Gellissen M, Palme H. Evidence for pervasive metamorphism on the CR chondrite parent body from highly equilibrated CR6 chondrites Northwest Africa 2994 and Northwest Africa 3100. *LPI*. 2008 :1991.
- Clayton RN, Mayeda TK. The oxygen isotope record in Murchison and other carbonaceous chondrites. *Earth Planet Sci Lett*. 1984; 67 :151–161.

- Clayton RN, Mayeda TK. Oxygen isotope studies of carbonaceous chondrites. *Geochim Cosmochim Acta*. 1999; 63 :2089–2104.
- Clayton RN, Mayeda TK, Goswami J, Olsen EJ. Oxygen isotope studies of ordinary chondrites. *Geochim Cosmochim Acta*. 1991; 55 :2317–2337.
- Clayton RN, Mayeda TK, Rubin AE. Oxygen isotopic compositions of enstatite chondrites and aubrites. *J Geophys Res Solid Earth*. 1984; 89 :C245–C249.
- Connelly JN, Bizzarro M, Krot AN, Nordlund A°, Wielandt D, Ivanova MA. The absolute chronology and thermal processing of solids in the solar protoplanetary disk. *Science*. 2012; 338 :651–655. [PubMed: 23118187]
- Dauphas N, Chen JH, Zhang J, Papanastassiou DA, Davis AM, Travaglio C. Calcium-48 isotopic anomalies in bulk chondrites and achondrites: evidence for a uniform isotopic reservoir in the inner protoplanetary disk. *Earth Planet Sci Lett*. 2014; 407 :96–108.
- Dauphas N, Remusat L, Chen J, Roskosz M, Papanastassiou D, Stodolna J, Guan Y, Ma C, Eiler J. Neutron-rich chromium isotope anomalies in supernova nanoparticles. *Astrophys J*. 2010; 720 :1577.
- Dunn TL, Gross J. Reclassification of Hart and Northwest Africa 6047: Criteria for distinguishing between CV and CK3 chondrites. *Meteorit Planet Sci*. 2017; 52 :2412–2423.
- Dunn TL, Gross J, Ivanova MA, Runyon SE, Bruck AM. Magnetite in the unequilibrated CK chondrites: Implications for metamorphism and new insights into the relationship between the CV and CK chondrites. *Meteorit Planet Sci*. 2016; 51 :1701–1720.
- Ebel DS, Brunner C, Konrad K, Leftwich K, Erb I, Lu M, Rodriguez H, Crapster-Pregont EJ, Friedrich JM, Weisberg MK. Abundance, major element composition and size of components and matrix in CV, CO and Acfer 094 chondrites. *Geochim Cosmochim Acta*. 2016; 172 :322–356.
- Elkins-Tanton LT, Weiss BP, Zuber MT. Chondrites as samples of differentiated planetesimals. *Earth Planet Sci Lett*. 2011; 305 :1–10.
- Eugster O. Cosmic-ray exposure ages of meteorites and lunar rocks and their significance. *Geochemistry*. 2003; 63 :3–30.
- Farquhar J, Thiemens MH, Jackson T. Atmosphere-surface interactions on Mars: D17O measurements of carbonate from ALH 84001. *Science*. 1998; 280 :1580–1582. [PubMed: 9616116]
- Fischer-Gödde M, Burkhardt C, Kruijer TS, Kleine T. Ru isotope heterogeneity in the solar protoplanetary disk. *Geochim Cosmochim Acta*. 2015; 168 :151–171.
- Fischer-Gödde M, Kleine T. Ruthenium isotope evidence for an inner Solar System origin of the late veneer. *Nature*. 2017; 541 :525. [PubMed: 28128236]
- Fujiya W, Sugiura N, Hotta H, Ichimura K, Sano Y. Evidence for the late formation of hydrous asteroids from young meteoritic carbonates. *Nat Commun*. 2012; 3 :627. [PubMed: 22252551]
- Fujiya W, Sugiura N, Sano Y, Hiyagon H. Mn-Cr ages of dolomites in CI chondrites and the Tagish Lake ungrouped carbonaceous chondrite. *Earth Planet Sci Lett*. 2013; 362 :130–142.
- Gattacceca J, Bonal L, Sonzogni C, Longerey J. CV chondrites: More than one parent body. *Earth Planet Sci Lett*. 2020; 547 :116467
- Gerber S, Burkhardt C, Budde G, Metzler K, Kleine T. Mixing and transport of dust in the early solar nebula as inferred from titanium isotope variations among chondrules. *Astrophys J Lett*. 2017; 841 :L17.
- Glavin D, Kubny A, Jagoutz E, Lugmair G. Mn-Cr isotope systematics of the D'Orbigny angrite. *Meteorit Planet Sci*. 2004; 39 :693–700.
- Glavin DP, Elsila JE, McLain HL, Aponte JC, Parker ET. Evidence for Extraterrestrial L-Amino Acid Excesses in the CM2 Aguas Zarcas and Murchison Carbonaceous Chondrites: Predictions for Ryugu and Bennu; 51st Lunar and Planetary Science Conference; 2020. 1025
- Göpel C, Birck J-L, Galy A, Barrat J-A, Zanda B. Mn-Cr systematics in primitive meteorites: Insights from mineral separation and partial dissolution. *Geochim Cosmochim Acta*. 2015; 156 :1–24.
- Gray C, Papanastassiou D, Wasserburg G. The identification of early condensates from the solar nebula. *Icarus*. 1973; 20 :213–239.
- Greenwood RC, Burbine TH, Miller MF, Franchi IA. Melting and differentiation of early-formed asteroids: The perspective from high precision oxygen isotope studies. *Chem Erde*. 2017; 77 :1–43.

- Greenwood RC, Franchi IA. Alteration and metamorphism of CO₃ chondrites: Evidence from oxygen and carbon isotopes. *Meteorit Planet Sci.* 2004; 39 :1823–1838.
- Greenwood RC, Franchi IA, Kearsley AT, Alard O. The relationship between CK and CV chondrites. *Geochim Cosmochim Acta.* 2010; 74 :1684–1705.
- Hans U, Kleine T, Bourdon B. Rb-Sr chronology of volatile depletion in differentiated protoplanets: BABI, ADOR and ALL revisited. *Earth Planet Sci Lett.* 2013; 374 :204–214.
- Hellmann JL, Hopp T, Burkhardt C, Kleine T. Origin of volatile element depletion among carbonaceous chondrites. *Earth Planet Sci Lett.* 2020; 549 :116508
- Hewins RH, Bourot-Denise M, Zanda B, Leroux H, Barrat J-A, Humayun M, Göpel C, Greenwood RC, Franchi IA, Pont S. The Paris meteorite, the least altered CM chondrite so far. *Geochim Cosmochim Acta.* 2014; 124 :190–222.
- Hezel DC, Russell SS, Ross AJ, Kearsley AT. Modal abundances of CAIs: Implications for bulk chondrite element abundances and fractionations. *Meteorit Planet Sci.* 2008; 43 :1879–1894.
- Holden NE. Total half-lives for selected nuclides. *Pure Appl Chem.* 1990; 62 :941–958.
- Inglis EC, Creech JB, Deng Z, Moynier F. High-precision zirconium stable isotope measurements of geological reference materials as measured by double-spike MC-ICPMS. *Chem Geol.* 2018; 493 :544–552.
- Ireland TR, Avila J, Greenwood RC, Hicks LJ, Bridges JC. Oxygen isotopes and sampling of the solar system. *Space Sci Rev.* 2020; 216 :25.
- Isa J, Rubin AE, Wasson JT. R-chondrite bulk chemical compositions and diverse oxides: Implications for parent-body processes. *Geochim Cosmochim Acta.* 2014; 124 :131–151.
- Javoy M, Kaminski E, Guyot F, Andraut D, Sanloup C, Moreira M, Labrosse S, Jambon A, Agrinier P, Davaille A. The chemical composition of the Earth: Enstatite chondrite models. *Earth Planet Sci Lett.* 2010; 293 :259–268.
- Jenniskens P, Fries MD, Yin Q-Z, Zolensky M, Krot AN, Sandford SA, Sears D, Beauford R, Ebel DS, Friedrich JM, Nagashima K, et al. Radar-enabled recovery of the Sutter's mill meteorite, a carbonaceous chondrite regolith breccia. *Science.* 2012; 338 :1583–1587. [PubMed: 23258889]
- Johansen A, Low M-M-M, Lacerda P, Bizzarro M. Growth of asteroids, planetary embryos, and Kuiper belt objects by chondrule accretion. *Sci Adv.* 2015; 1 e1500109 [PubMed: 26601169]
- Kadlag Y, Becker H, Harbott A. Cr isotopes in physically separated components of the Allende CV3 and Murchison CM2 chondrites: Implications for isotopic heterogeneity in the solar nebula and parent body processes. *Meteorit Planet Sci.* 2019; 54 :2116–2131.
- Kallemeyn GW, Rubin AE, Wasson JT. The compositional classification of chondrites: V. The Karoonda (CK) group of carbonaceous chondrites. *Geochim Cosmochim Acta.* 1991; 55 :881–892.
- Kallemeyn GW, Wasson JT. The compositional classification of chondrites—I. The carbonaceous chondrite groups. *Geochim Cosmochim Acta.* 1981; 45 :1217–1230.
- Koeberl C, Shukolyukov A, Lugmair GW. Chromium isotopic studies of terrestrial impact craters: Identification of meteoritic components at Bosumtwi, Clearwater East, Lap-pajärvi, and Rochechouart. *Earth Planet Sci Lett.* 2007; 256 :534–546.
- Krot AN, Amelin Y, Cassen P, Meibom A. Young chondrules in CB chondrites from a giant impact in the early solar system. *Nature.* 2005; 436 :989–992. [PubMed: 16107841]
- Krot, AN, Keil, K, Scott, ERD, Goodrich, CA, Weisberg, MK. 1.1 – Classification of meteorites and their genetic relationships A2 – Holland, Heinrich D Treatise on Geochemistry. second. Turekian, KK, editor. Elsevier; Oxford: 2014. 1–63.
- Krot AN, Meibom A, Keil K. A clast of Bali-like oxidized CV material in the reduced CV chondrite breccia Vigarano. *Meteorit Planet Sci.* 2000; 35 :817–825.
- Krot AN, Nagashima K. Constraints on mechanisms of chondrule formation from chondrule precursors and chronology of transient heating events in the protoplanetary disk. *Geochem J.* 2017; 51 :45–68.
- Krot AN, Petaev MI, Scott ER, Choi BG, Zolensky ME, Keil K. Progressive alteration in CV3 chondrites: More evidence for asteroidal alteration. *Meteorit Planet Sci.* 1998; 33 :1065–1085.
- Kruijjer TS, Borg LE, Wimpenny J, Sio CK. Onset of magma ocean solidification on Mars inferred from Mn-Cr chronometry. *Earth Planet Sci Lett.* 2020; 542 :116315

- Langbroek M, Jenniskens P, Kriegsman LM, Nieuwenhuis H, De Kort N, Kuiper J, Van Westrenen W, Zolensky ME, Ziegler, Yin QZ. The CM carbonaceous chondrite regolith Diepenveen. *Meteorit Planet Sci.* 2019; 54 :1431–1461.
- Larsen KK, Trinquier A, Paton C, Schiller M, Wielandt D, Ivanova MA, Connelly JN, Nordlund A, Krot AN, Bizzarro M. Evidence for magnesium isotope heterogeneity in the solar protoplanetary disk. *Astrophys J Lett.* 2011; 735 :L37.
- Larsen K K, Wielandt D, Bizzarro M. Multi-element-exchange chromatography and high-precision MC-ICP-MS isotope analysis of Mg and Ti from sub-mm-sized meteorite inclusions. *J Anal At Spectrom.* 2018; 33 :613–628.
- Larsen KK, Wielandt D, Schiller M, Bizzarro M. Chromatographic speciation of Cr(III)-species, inter-species equilibrium isotope fractionation and improved chemical purification strategies for high-precision isotope analysis. *J Chromatogr A.* 2016; 1443 :162–174. [PubMed: 27036208]
- Li S, Yin Q-Z, Bao H, Sanborn ME, Irving A, Ziegler K, Agee C, Marti K, Miao B, Li X, Li Y, et al. Evidence for a multilayered internal structure of the chondritic acapulcoite-lodranite parent asteroid. *Geochim Cosmochim Acta.* 2018; 242 :82–101.
- Lodders, K, Fegley, B, Lodders, F. *The planetary scientist's companion.* Oxford University Press on Demand; 1998.
- Lugmair G, Shukolyukov A. Early solar system timescales according to ^{53}Mn - ^{53}Cr systematics. *Geochim Cosmochim Acta.* 1998; 62 :2863–2886.
- Magna T, Zák K, Pack A, Moynier F, Mougél B, Peters S, Skaála R, Jonaášová S, Mizera J, Ránda Z. Zhamanshin astrobleme provides evidence for carbonaceous chondrite and post-impact exchange between ejecta and Earth's atmosphere. *Nat Commun.* 2017; 8 :227. [PubMed: 28794408]
- Mahan B, Moynier F, Siebert J, Gueguen B, Agranier A, Pringle EA, Bollard J, Connelly JN, Bizzarro M. Volatile element evolution of chondrules through time. *Proc Natl Acad Sci.* 2018; 115 :201807263
- Mann U, Frost DJ, Rubie DC. Evidence for high-pressure core-mantle differentiation from the metal-silicate partitioning of lithophile and weakly-siderophile elements. *Geochim Cosmochim Acta.* 2009; 73 :7360–7386.
- Mougél B, Moynier F, Göpel C. Chromium isotopic homogeneity between the Moon, the Earth, and enstatite chondrites. *Earth Planet Sci Lett.* 2018; 481 :1–8.
- Mougél B, Moynier F, Göpel C, Koeberl C. Chromium isotope evidence in ejecta deposits for the nature of Paleoproterozoic impactors. *Earth Planet Sci Lett.* 2017; 460 :105–111.
- Mougél B, Moynier F, Koeberl C, Wielandt D, Bizzarro M. Identification of a meteoritic component using chromium isotopic composition of impact rocks from the Lonar impact structure, India. *Meteorit Planet Sci.* 2019; 54 :2592–2599.
- Moynier F, Day JM, Okui W, Yokoyama T, Bouvier A, Walker RJ, Podosek FA. Planetary-scale strontium isotopic heterogeneity and the age of volatile depletion of early Solar System materials. *Astrophys J.* 2012; 758 :45.
- Moynier F, Yin Q-Z, Jacobsen B. Dating the first stage of planet formation. *Astrophys J Lett.* 2007; 671 :L181.
- Newton J, Franchi IA, Pillinger CT. The oxygen isotopic record in enstatite meteorites. *Meteorit Planet Sci.* 2000; 35 :689–698.
- Nittler LR, Alexander CMD, Liu N, Wang J. Extremely ^{54}Cr - and ^{50}Ti -rich presolar oxide grains in a primitive meteorite: Formation in rare types of supernovae and implications for the astrophysical context of solar system birth. *Astrophys J Lett.* 2018; 856 :L24. [PubMed: 31049193]
- Nyquist L, Lindstrom D, Mittlefehldt D, Shih CY, Wiesmann H, Wentworth S, Martinez R. Manganese-chromium formation intervals for chondrules from the Bishunpur and Chainpur meteorites. *Meteorit Planet Sci.* 2001; 36 :911–938.
- Olsen MB, Wielandt D, Schiller M, Van Kooten EMME, Bizzarro M. Magnesium and ^{54}Cr isotope compositions of carbonaceous chondrite chondrules – Insights into early disk processes. *Geochim Cosmochim Acta.* 2016; 191 :118–138. [PubMed: 27563152]
- Palme, H, O'Neill, HSC. 3.1 – Cosmochemical estimates of mantle composition *Treatise on Geochemistry*, second. Holland, HD, Turekian, KK, editors. Elsevier; Oxford: 2014. 1–39.

- Pedersen SG, Schiller M, Connelly JN, Bizzarro M. Testing accretion mechanisms of the H chondrite parent body utilizing nucleosynthetic anomalies. *Meteorit Planet Sci.* 2019; 54 :1215–1227.
- Petit M, Birck J-L, Luu T, Gounelle M. The chromium isotopic composition of the ungrouped carbonaceous chondrite Tagish Lake. *Astrophys J.* 2011; 736 :23.
- Piani L, Marrocchi Y, Libourel G, Tissandier L. Magmatic sulfides in the porphyritic chondrules of EH enstatite chondrites. *Geochim Cosmochim Acta.* 2016; 195 :84–99.
- Piani L, Marrocchi Y, Rigaudier T, Vacher LG, Thomassin D, Marty B. Earth's water may have been inherited from material similar to enstatite chondrite meteorites. *Science.* 2020; 369 :1110–1113. [PubMed: 32855337]
- Podosek F, Ott U, Brannon J, Neal C, Bernatowicz T, Swan P, Mahan S. Thoroughly anomalous chromium in Orgueil. *Meteorit Planet Sci.* 1997; 32 :617–627.
- Popovas A, Nordlund A°, Ramsey JP, Ormel CW. Pebble dynamics and accretion on to rocky planets-I. Adiabatic and convective models. *MNRAS.* 2018; 479 :5136–5156.
- Qin L, Alexander CMOD, Carlson RW, Horan MF, Yokoyama T. Contributors to chromium isotope variation of meteorites. *Geochim Cosmochim Acta.* 2010; 74 :1122–1145.
- Qin L, Nittler LR, Alexander CMOD, Wang J, Stadermann FJ, Carlson RW. Extreme ⁵⁴Cr-rich nano-oxides in the CI chondrite Orgueil – Implication for a late supernova injection into the solar system. *Geochim Cosmochim Acta.* 2011; 75 :629–644.
- Rotaru M, Birck JL, Allègre CJ. Clues to early solar system history from chromium isotopes in carbonaceous chondrites. *Nature.* 1992; 358 :465.
- Rubin AE, Fegley B, Brett R. Oxidation state in chondrites. *Meteorit Early Solar Syst.* 1988 :488–511.
- Rubin, AE, Kallemeyn, GW, Wasson, JT, Clayton, RN, Mayeda, TK, Grady, M, Verchovsky, A. Gujba: A new Bencubbin-like meteorite fall from Nigeria. *LPI Contributions*; 2001. 1779
- Sanborn ME, Wimpenny J, Williams CD, Yamakawa A, Amelin Y, Irving AJ, Yin Q-Z. Carbonaceous chondrites Northwest Africa 6704/6693: Milestones for early solar system chronology and genealogy. *Geochim Cosmochim Acta.* 2019; 245 :577–596.
- Scherer P, Schultz L. Noble gas record, collisional history, and pairing of CV, CO, CK, and other carbonaceous chondrites. *Meteorit Planet Sci.* 2000; 35 :145–153.
- Schiller M, Bizzarro M, Fernandes VA. Isotope evolution of the protoplanetary disk and the building blocks of Earth and the Moon. *Nature.* 2018; 555 :507. [PubMed: 29565359]
- Schiller M, Bizzarro M, Siebert J. Iron isotope evidence for very rapid accretion and differentiation of the proto-Earth. *Sci Adv.* 2020; 6 eaay7604 [PubMed: 32095530]
- Schiller M, Van Kooten E, Holst JC, Olsen MB, Bizzarro M. Precise measurement of chromium isotopes by MC-ICPMS. *J Anal At Spectrom.* 2014; 29 :1406–1416. [PubMed: 25071300]
- Schmitz B, Yin Q-Z, Sanborn M, Tassinari M, Caplan C, Huss G. A new type of solar-system material recovered from Ordovician marine limestone. *Nat Commun.* 2016; 7 ncomms11851 [PubMed: 27299793]
- Schneider JM, Burkhardt C, Marrocchi Y, Brennecka GA, Kleine T. Early evolution of the solar accretion disk inferred from Cr-Ti-O isotopes in individual chondrules. *Earth Planet Sci Lett.* 2020; 551 :116585
- Schrader DL, Davidson J. CM and CO chondrites: A common parent body or asteroidal neighbors? Insights from chondrule silicates. *Geochim Cosmochim Acta.* 2017; 214 :157–171.
- Schrader DL, Davidson J, Greenwood RC, Franchi IA, Gibson JM. A water-ice rich minor body from the early Solar System: The CR chondrite parent asteroid. *Earth Planet Sci Lett.* 2014; 407 :48–60.
- Schrader DL, Franchi IA, Connolly HC, Greenwood RC, Lauretta DS, Gibson JM. The formation and alteration of the Renazzo-like carbonaceous chondrites I: Implications of bulk-oxygen isotopic composition. *Geochim Cosmochim Acta.* 2011; 75 :308–325.
- Scott, ER, Krot, AN. Chondritic meteorites and the high-temperature nebular origins of their components. *Chondrites and the Protoplanetary Disk.* 2005. 15
- Shukolyukov A, Lugmair G. Manganese-chromium isotope systematics of carbonaceous chondrites. *Earth Planet Sci Lett.* 2006; 250 :200–213.

- Sossi P, Moynier F, van Zuilen K. Volatile loss following cooling and accretion of the Moon revealed by chromium isotopes. *Proc Natl Acad Sci*. 2018; 115 :10920–10925. [PubMed: 30297398]
- Sossi A, Klemme S, O'Neill H SC, Berndt J, Moynier F. Evaporation of moderately volatile elements from silicate melts: experiments and theory. *Geochim Cosmochim Acta*. 2019; 260 :204–231.
- Spitzer F, Burkhardt C, Budde G, Kruijer TS, Morbidelli A, Kleine T. Isotopic evolution of the inner solar system inferred from molybdenum isotopes in meteorites. *Astrophys J Lett*. 2020; 898 :L2.
- Steele RCJ, Elliott T, Coath CD, Regelous M. Confirmation of mass-independent Ni isotopic variability in iron meteorites. *Geochim Cosmochim Acta*. 2011; 75 :7906–7925.
- Steele RC, Coath CD, Regelous M, Russell S, Elliott T. Neutron-poor nickel isotope anomalies in meteorites. *Astrophys J*. 2012; 758 :59.
- Stracke A, Palme H, Gellissen M, Münker C, Kleine T, Birbaum K, Günther D, Bourdon B, Zipfel J. Refractory element fractionation in the Allende meteorite: Implications for solar nebula condensation and the chondritic composition of planetary bodies. *Geochim Cosmochim Acta*. 2012; 85 :114–141.
- Sugiura N, Fujiya W. Correlated accretion ages and ^{54}Cr of meteorite parent bodies: the evolution of the solar nebula. *Meteorit Planet Sci*. 2014; 49 :772–787.
- Sun S-S. Chemical composition and origin of the Earth's primitive mantle. *Geochim Cosmochim Acta*. 1982; 46 :179–192.
- Trinquier A, Birck J-L, Allègre CJ. The nature of the KT impactor. A ^{54}Cr reappraisal. *Earth Planet Sci Lett*. 2006; 241 :780–788.
- Trinquier A, Birck J-L, Allègre CJ. Widespread ^{54}Cr heterogeneity in the inner solar system. *Astrophys J*. 2007; 655 :1179–1185.
- Trinquier A, Birck J-L, Allègre CJ. High-precision analysis of chromium isotopes in terrestrial and meteorite samples by thermal ionization mass spectrometry. *J Anal At Spectrom*. 2008a; 23 :1565–1574.
- Trinquier A, Birck JL, Allègre CJ, Göpel C, Ulfbeck D. ^{53}Mn - ^{53}Cr systematics of the early Solar System revisited. *Geochim Cosmochim Acta*. 2008b; 72 :5146–5163.
- Trinquier A, Elliott T, Ulfbeck D, Coath C, Krot AN, Bizzarro M. Origin of nucleosynthetic isotope heterogeneity in the solar protoplanetary disk. *Science*. 2009; 324 :374–376. [PubMed: 19372428]
- van Kooten E, Cavalcante L, Wielandt D, Bizzarro M. The role of Bells in the continuous accretion between the CM and CR chondrite reservoirs. *Meteorit Planet Sci* n/a. 2020
- Van Kooten EMME, Wielandt D, Schiller M, Nagashima K, Thomen A, Larsen KK, Olsen MB, Nordlund A°, Krot A N, Bizzarro M. Isotopic evidence for primordial molecular cloud material in metal-rich carbonaceous chondrites. *Proc Natl Acad Sci*. 2016; 113 :2011–2016. [PubMed: 26858438]
- Vermeesch P. IsoplotR: A free and open toolbox for geochronology. *Geosci Front*. 2018; 9 :1479–1493.
- Visscher C, Fegley B Jr. Chemistry of impact-generated silicate melt-vapor debris disks. *Astrophys J Lett*. 2013; 767 :L12.
- Wadhwa M, Shukolyukov A, Davis AM, Lugmair GW, Mittlefehldt DW. Differentiation history of the mesosiderite parent body: constraints from trace elements and manganese-chromium isotope systematics in Vaca Muerta silicate clasts. *Geochim Cosmochim Acta*. 2003; 67 :5047–5069.
- Wang HS, Lineweaver CH, Ireland TR. The elemental abundances (with uncertainties) of the most Earthlike planet. *Icarus*. 2018; 299 :460–474.
- Wang K, Moynier F, Podosek F, Foriel J. ^{58}Fe and ^{54}Cr in early solar system materials. *Astrophys J Lett*. 2011; 739 :L58.
- Wänke H, Dreibus G. Chemical composition and accretion history of terrestrial planets. *Phil Trans R Soc Lond A*. 1988; 325 :545–557.
- Warren PH. Stable-isotopic anomalies and the accretionary assemblage of the Earth and Mars: A subordinate role for carbonaceous chondrites. *Earth Planet Sci Lett*. 2011; 311 :93–100.
- Wasson JT, Isa J, Rubin AE. Compositional and petrographic similarities of CV and CK chondrites: A single group with variations in textures and volatile concentrations attributable to impact heating, crushing and oxidation. *Geochim Cosmochim Acta*. 2013; 108 :45–62.

- Weber HW, Franke L, Schultz L. Subsolar noble gases in metal-rich carbonaceous (CH) chondrites. *Meteorit Planet Sci.* 2001; 36 :A220
- Weisberg MK, McCoy TJ, Krot AN. Systematics and evaluation of meteorite classification. *Meteorites and the Early Solar System II.* 2006
- Weisberg MK, Prinz M, Clayton RN, Mayeda TK, Sugiura N, Zashu S, Ebihara M. A new metal-rich chondrite grouplet. *Meteorit Planet Sci.* 2001; 36 :401–418.
- Williams CD, Sanborn ME, Defouilloy C, Yin Q-Z, Kita NT, Ebel DS, Yamakawa A, Yamashita K. Chondrules reveal large-scale outward transport of inner Solar System materials in the protoplanetary disk. *Proc Natl Acad Sci.* 2020; 117 :23426–23435.
- Yamakawa A, Yamashita K, Makishima A, Nakamura E. Chromium isotope systematics of achondrites: Chronology and isotopic heterogeneity of the inner solar system bodies. *Astrophys J.* 2010; 720 :150.
- Yamashita K, Maruyama S, Yamakawa A, Nakamura E. ^{53}Mn - ^{53}Cr chronometry of CB chondrite: Evidence for uniform distribution of ^{53}Mn in the early solar system. *Astrophys J.* 2010; 723 :20.
- Yokoyama T, Nagai Y, Fukai R, Hirata T. Origin and evolution of distinct molybdenum isotopic variabilities within carbonaceous and noncarbonaceous reservoirs. *Astrophys J.* 2019; 883 :62.
- Young ED, Galy A. The isotope geochemistry and cosmochemistry of magnesium. *Rev Mineral Geochem.* 2004; 55 :197–230.
- Zhang J, Dauphas N, Davis AM, Leya I, Fedkin A. The proto-Earth as a significant source of lunar material. *Nat Geosci.* 2012; 5 :251–255.
- Zhu K, Liu J, Moynier F, Qin L, Alexander CMOD, He Y. Chromium isotopic evidence for an early formation of chondrules from the Ornans CO chondrite. *Astrophys J.* 2019a; 873 :82.
- Zhu K, Moynier F, Barrat J-A, Wielandt D, Larsen K, Bizzarro M. Timing and origin of the angrite parent body inferred from Cr isotopes. *Astrophys J Lett.* 2019b; 877 :L13.
- Zhu K, Moynier F, Schiller M, Alexander CMOD, Barrat J-A, Bischoff A, Bizzarro M. Mass-independent and mass-dependent Cr isotopic composition of the Rumuruti (R) chondrites: Implications for their origin and planet formation. *Geochim Cosmochim Acta.* 2021; 293 :598–609.
- Zhu K, Moynier F, Schiller M, Bizzarro M. Dating and tracing the origin of enstatite chondrite chondrules with Cr isotopes. *Astrophys J Lett.* 2020a; 894 :L26.
- Zhu K, Moynier F, Schiller M, Wielandt D, Larsen K, van Kooten E, Bizzarro M. Chromium isotopic constraints on the origin of the ureilite parent body. *Astrophys J.* 2020b; 888 :126.
- Zhu K, Sossi PA, Siebert J, Moynier F. Tracking the volatile and magmatic history of Vesta from chromium stable isotope variations in eucrite and diogenite meteorites. *Geochim Cosmochim Acta.* 2019c; 266 :598–610.

The $\epsilon^{54}\text{Cr}$ Variation in Chondrites

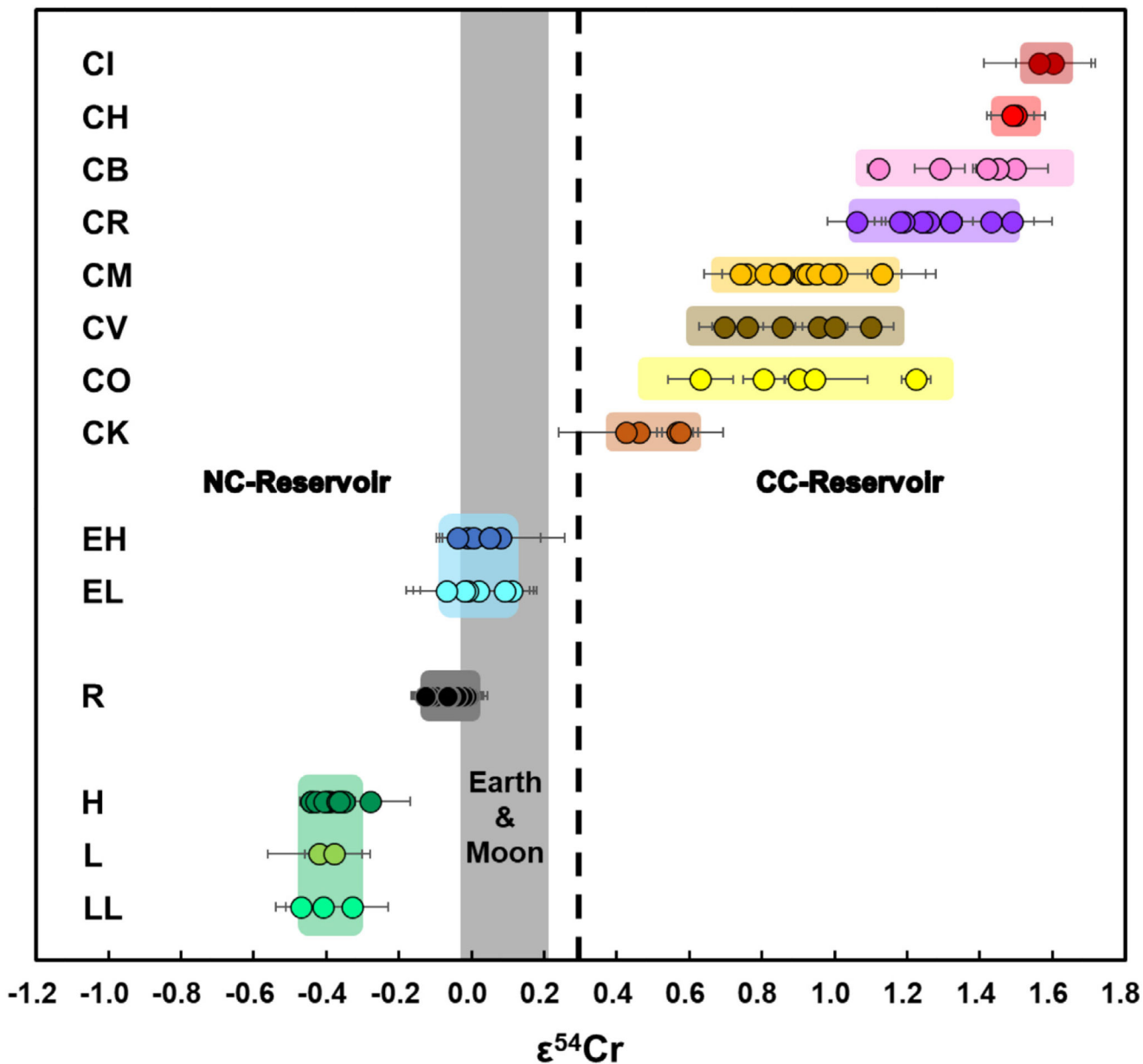


Fig. 1. The $\epsilon^{54}\text{Cr}$ variations in different groups of chondrites (the data and reference sources can be found in Tables 4–6), which occur in the order CI = CH CB CR > CM \approx CV \approx CO CK > EC \approx RC > OC. The color shades indicate the 2SD variation of different chondrite groups (the blue and green shades show the 2SD uncertainty of all the ECs and OCs respectively; we use the external reproducibility 0.07 to represent the grouping uncertainties of CIs and CHs since the 2SD uncertainty are less than 0.07). The middle bold dashed line at $\epsilon^{54}\text{Cr} = +0.3$ is the $\epsilon^{54}\text{Cr}$ boundary for non-carbonaceous chondrite (NC) and carbonaceous chondrite (CC) reservoirs. All CK, RC, OC and EC groups have homogeneous $\epsilon^{54}\text{Cr}$ within

their respective groups. The CV and CK chondrites have distinct $\epsilon^{54}\text{Cr}$ values from one another, whereas the $\epsilon^{54}\text{Cr}$ for CV, CM and CO chondrites overlap. EC and RC have similar $\epsilon^{54}\text{Cr}$ features with the Earth-Moon system.

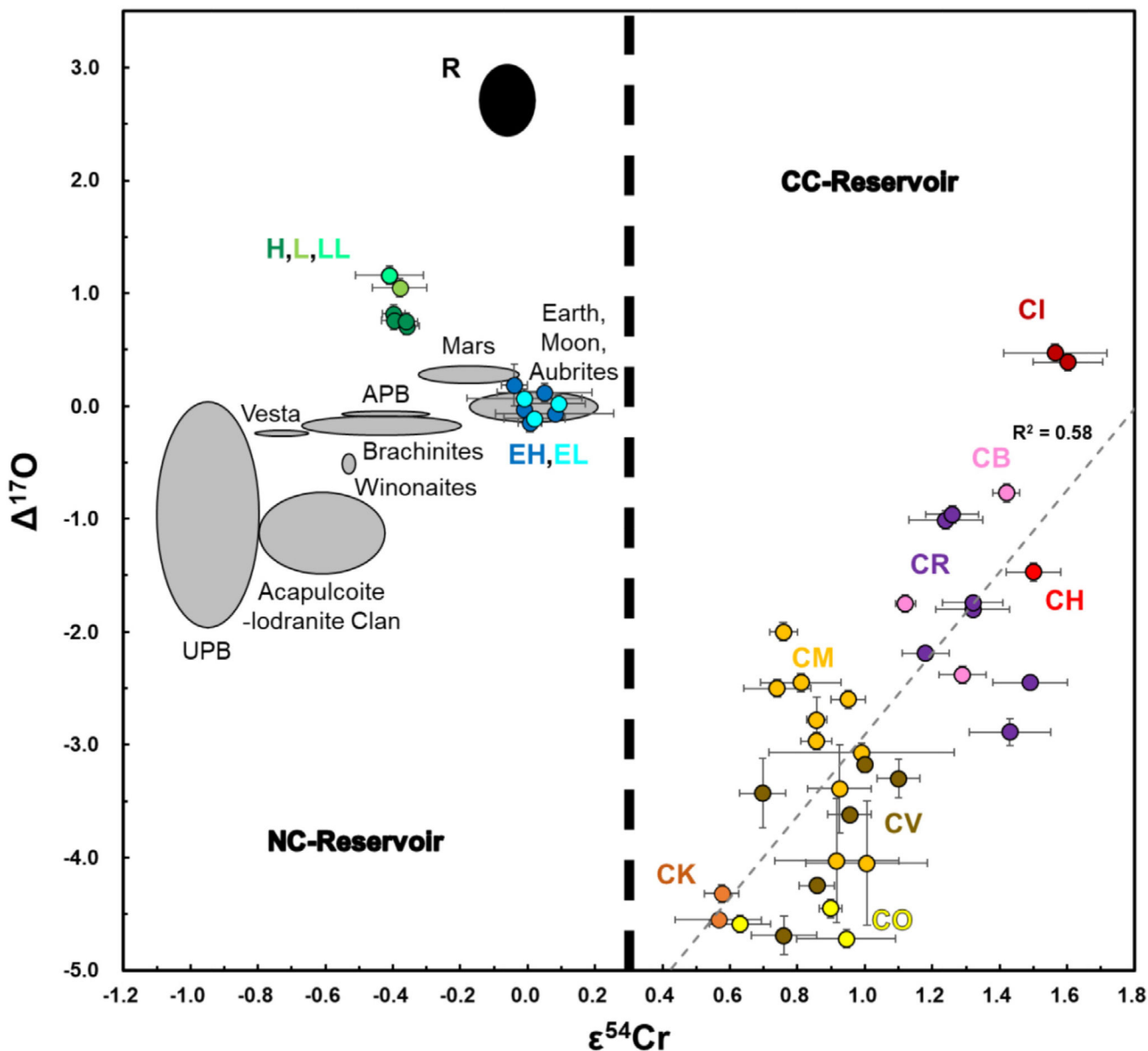


Fig. 2. The $\epsilon^{54}\text{Cr}$ and $\Delta^{17}\text{O}$ compositions of the CCs, OCs, ECs (filled circles), as well as achondrites, terrestrial and lunar samples (gray ellipses). The data sources for planets and achondrites are shown in Table 5. NC: non-CCs; APB: angrite parent body; UPB: ureilite parent body. The colored circles represent the same samples that are shown in Fig. 1. It should be noted that the correlation between $\epsilon^{54}\text{Cr}$ and $\Delta^{17}\text{O}$ values in CCs is not as strong ($R^2=0.58$) as that described in Trinquier et al. (2007) and Warren (2011). The $\epsilon^{54}\text{Cr}$ gap between the CC and NC reservoirs is +0.3, because some terrestrial samples and the ECs have $\epsilon^{54}\text{Cr}$ values in the range 0 - 0.2, and no CCs possess $\epsilon^{54}\text{Cr}$ values < 0.4.

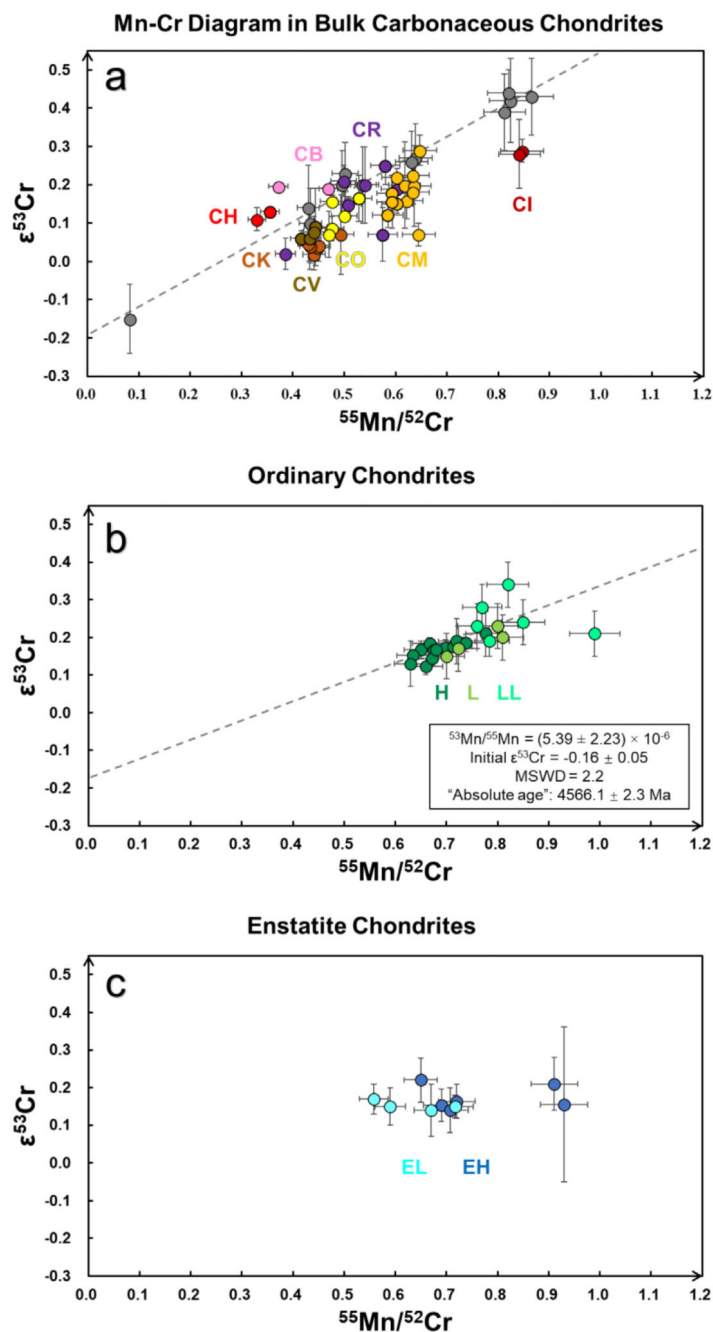
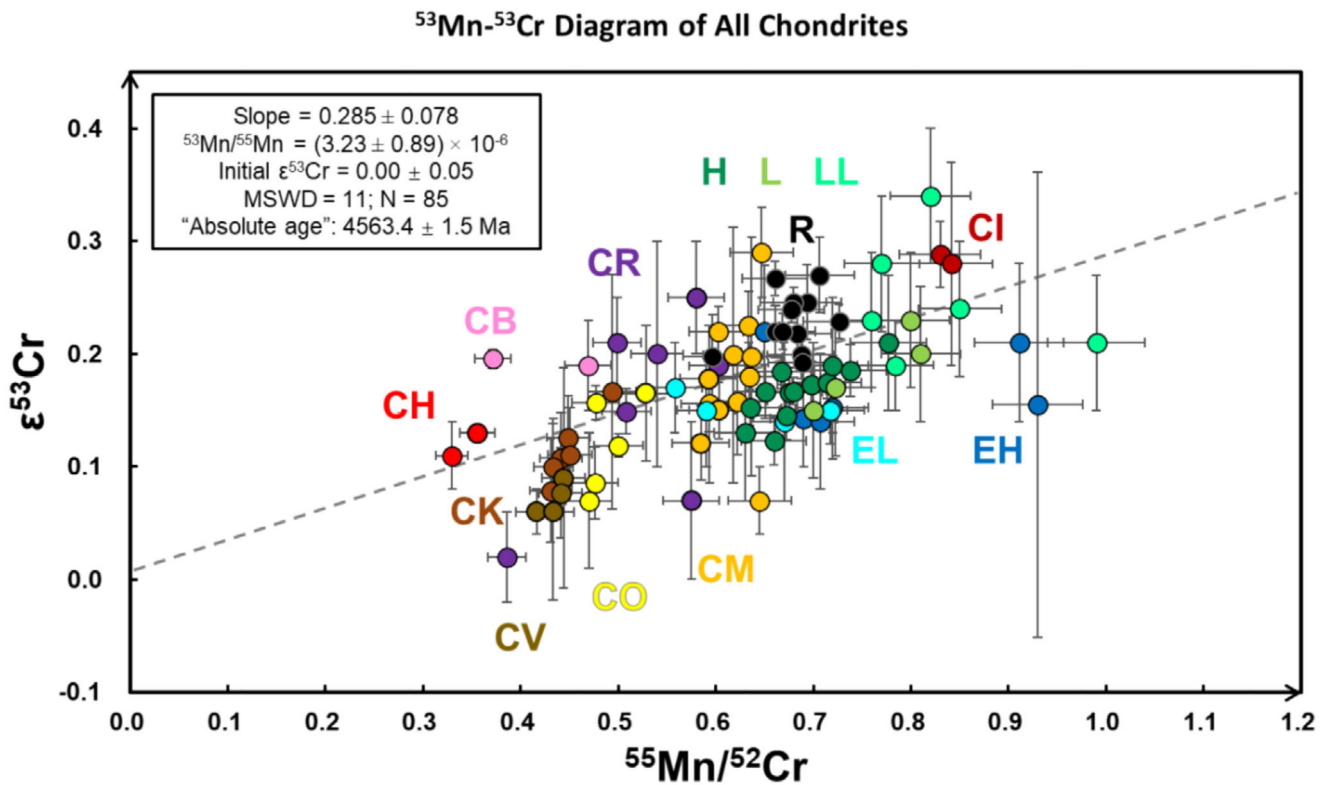
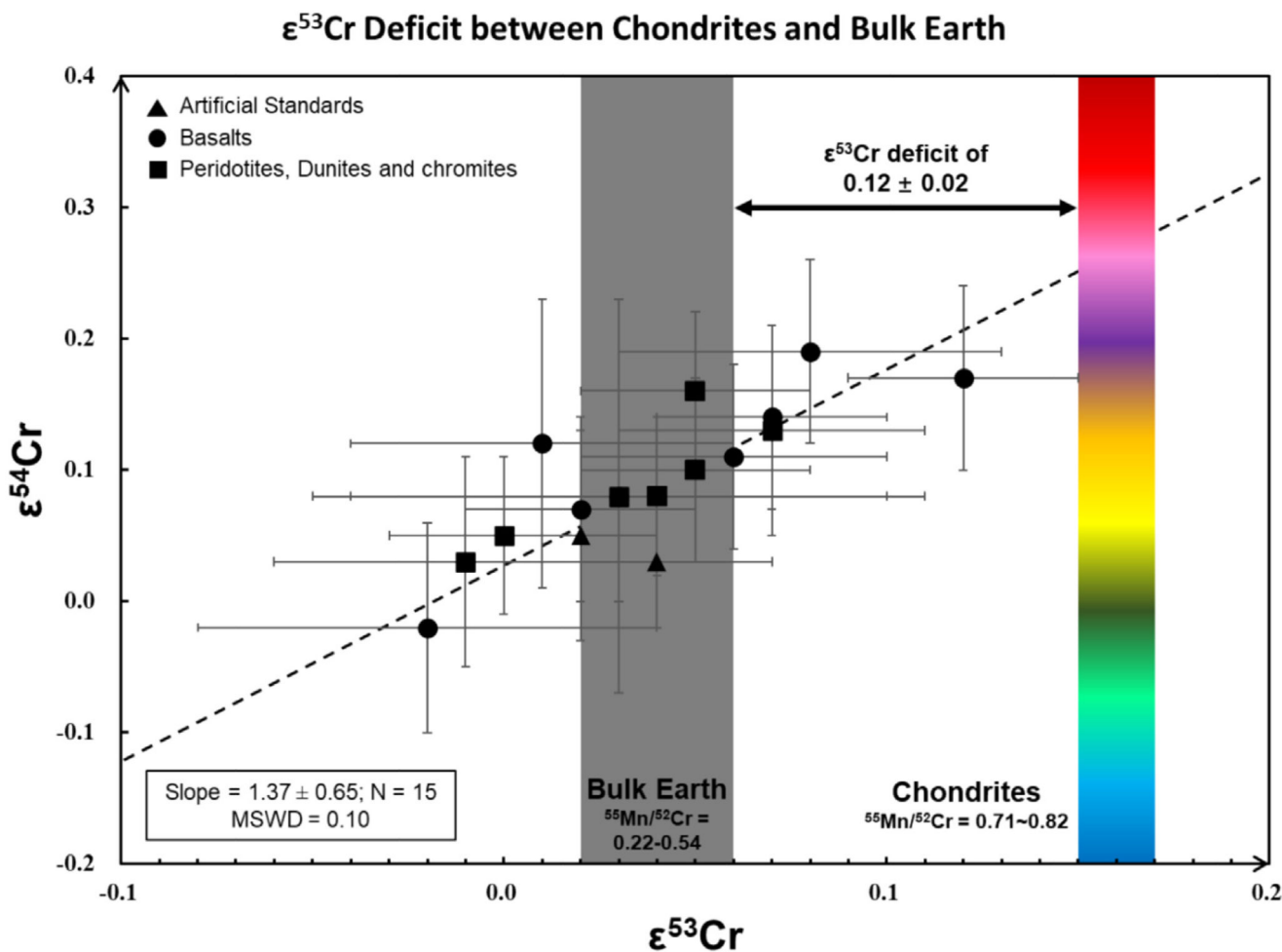


Fig. 3. $^{55}\text{Mn}/^{52}\text{Cr}$ vs. $\epsilon^{53}\text{Cr}$ in the CCs (a), OCs (b) and ECs (c).

In (a), the gray circles and dashed line are from Moynier et al. (2007) and Shukolyukov and Lugmair (2006), who reported well-defined ^{53}Mn - ^{53}Cr isochrons. However, the additional data presented here (colored data points; the colors for chondrite groups are the same as in Fig. 1) do not reproduce this correlation line. (a) Does not include the ^{53}Mn - ^{53}Cr data for the silicate parts of CB chondrites. The best fit ^{53}Mn - ^{53}Cr correlation line in (b) may be a mixing line rather than an isochron.

**Fig. 4.**

All of the $^{55}\text{Mn}/^{52}\text{Cr}$ and $\epsilon^{53}\text{Cr}$ data for the different chondrite groups. The warm-color circles are the CCs, while the black, green and blue ones are the RCs, OCs and ECs, respectively. The data are from Table 4, and regressed by Model 3 (maximum likelihood regression with overdispersion), *Isoplot R* (Vermeesch, 2018). This figure does not include the ^{53}Mn - ^{53}Cr data for the silicate parts of CB chondrites. There is a positive trend (gray dashed line) between $^{55}\text{Mn}/^{52}\text{Cr}$ and $\epsilon^{53}\text{Cr}$ with a slope of 0.285 ± 0.078 (MSWD = 11, N = 85; some literature data do not have $^{55}\text{Mn}/^{52}\text{Cr}$ ratio information) regressed by model 3, *Isoplot R*. This ^{53}Mn - ^{53}Cr correlation line is interpreted as a mixing trend and, as such, does not have chronological significance.

**Fig. 5.**

The $\epsilon^{53}\text{Cr}$ and $\epsilon^{54}\text{Cr}$ values for terrestrial rocks (Table 5) and chondrites. The black circles and squares are terrestrial crustal and mantle rocks respectively, while the black triangles are artificial standards (i.e., NIST SRM 3112a and SCP-Cr). The $\epsilon^{53}\text{Cr}$ and $\epsilon^{54}\text{Cr}$ values for terrestrial rocks are correlated with a slope of 1.37 ± 0.65 ($N = 15$, $\text{MSWD} = 0.1$), regressed by Model 1, *Isoplot R* (Vermeesch, 2018). This correlation indicates the residual mass-dependent Cr isotope fractionation. The gray and colorful bars indicate the average $\epsilon^{53}\text{Cr}$ values (with 2SE uncertainty) for bulk silicate Earth (BSE; $N = 15$) and chondrites ($N = 88$), respectively. The two artificial standards are not considered to represent the Cr isotope composition of Earth. There is a $\epsilon^{53}\text{Cr}$ deficit of 0.12 ± 0.02 between BE and chondrites, which potentially indicate an early volatile fractionation of proto-Earth. The $^{55}\text{Mn}/^{52}\text{Cr}$ for BE of 0.22-0.54, was estimated by Sun (1982), Wang et al. (2018), Wänke and Dreibus (1988) and (Palme and O'Neill, 2014), while the $^{55}\text{Mn}/^{52}\text{Cr}$ for chondrites are from those of the ECs (0.71; having the same isotope compositions with Earth for multiple elements) and CIs (0.82; are regarded to represent the chemical composition of the Solar System). In this figure, $^{55}\text{Mn}/^{52}\text{Cr}$ ratios of 0.71-0.82 are only from ECs and CI chondrites, but note that some other groups of chondrites (e.g., CV, CO and CK in Fig. 4) may have

an Earth-like $^{55}\text{Mn}/^{52}\text{Cr}$ ratios. No systematic differences were observed in data measured by MC-ICP-MS in this study and by TIMS in the literature. isotope-corrected D'Orbigny angrite. However, this ^{53}Mn - ^{53}Cr correlation line likely represent a mixing line that does not have any chronological significance.

Calculated $\Delta^{53}\text{Cr}$ and $\Delta^{54}\text{Cr}$ using different Cr oxides and different fractionation laws

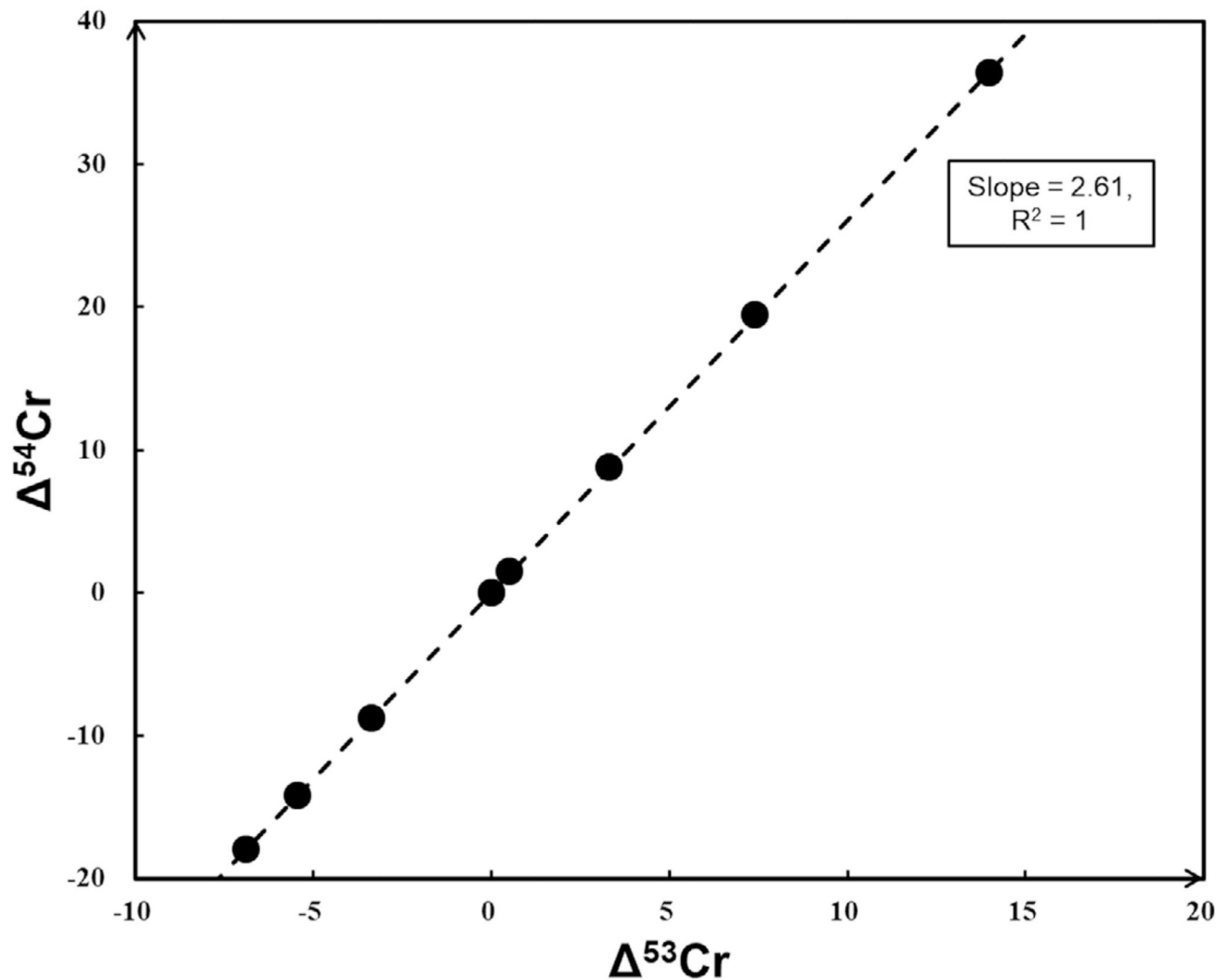


Fig. 6. Calculated $\Delta^{53}\text{Cr}$ and $\Delta^{54}\text{Cr}$ (for evaporation of only Cr^+ by kinetic isotope fractionation) using different Cr oxides (CrO , CrO_2 and CrO_3) and different fractionation laws (kinetic and equilibrium). The data sources are from Tables 7a and 7b. It should be noted that the variation factor (slope) between $\Delta^{53}\text{Cr}$ and $\Delta^{54}\text{Cr}$ is 2.61 that is highly consistent with the slope (2.6) between $\epsilon^{53}\text{Cr}$ and $\epsilon^{54}\text{Cr}$ values of multiple measurements for NIST 3112a (Qin et al., 2010).

Table 1
Four-step column chemistry used in this study to purify chromium.

Eluent	Volume (ml)	Procedural step	Elements eluted
Step 1: 0.5 ml Biorad AG1-X8 200-400 mesh resin			
6M HCl	2	Condition	
6M HCl	0.5	Sample Load	
6M HCl	3	Cr collection	Cr + matrix
H ₂ O	5	Wash	Fe + Ni
Step 2: 1 ml Biorad AG50W-X8 200-400 mesh resin			
0.5 M HCl	3	Condition	
0.5 M HCl	3	*1 Sample Load	
0.5 M HNO ₃	20	Cr collection	Cr + matrix
6M HCl	5	Wash	Mg +; Ca + Al +; Mn + Ni
Step 3: 0.33 ml Biorad AG50W-X8 200-400 mesh resin			
H ₂ O	1	Condition	
0.5 M HNO ₃	0.5	*2 Sample Load and Cr collection	Cr
0.5 M HNO ₃	0.5	Cr collection	Cr
1M HF	2.5	Matrix elution	Ti + V + K + Na + Fe + Al
1M HCl	6	Matrix elution	K+ Na
6M HCl	3	Cr collection + Wash	Cr
Step 4: 0.75 ml Eichrom TODGA resin			
8M HCl	2	Condition	
8M HCl	0.5	Sample Load	Cr
8M HCl	2	Cr collection	Cr
H ₂ O	4	Wash	V + Fe + Ti

*1 Note: Sample pretreatment: dissolving sample in 0.25 ml 6 M HCl (in 7 ml beaker) with heating at >120 °C for more than 2 h, then added 2.75 ml H₂O before loading. This is to transform Cr as Cr⁰

*2 Sample pretreatment: dissolving sample in 0.125 ml 2 M HNO₃ (in 3 ml beaker) with heating at 100 °C for 2 h, then added 0.01 ml H₂O₂ and 0.365 ml H₂O, and put the mixture at room temperature for more than 24 h. This is to maximize the oxidation of Cr as Cr³⁺.

Table 2
Doping test for V, Ti, Fe, Na and K and external precision tests by Allende, DTS-1 and Orgueil.

Samples	Interference Contribution (ppm)*	$e^{53}\text{Cr}$	2se	$e^{54}\text{Cr}$	2se	N[ref.]
Cr-V-0%	0	0.00	0.00	-0.01	0.02	5
Cr-V-S14	24	0.00	0.02	0.00	0.02	[1]
Cr-V-0.5%	269	0.00	0.03	0.04	0.02	5
Cr-V-2.5%	1438	-0.06	0.02	-0.07	0.03	5
Cr-V-5%	2764	-0.09	0.01	-0.12	0.04	5
Cr-Ti-0%	0	-0.01	0.02	0.02	0.03	5
Cr-Ti-S14	1609	0.01	0.02	0.00	0.02	[1]
Cr-Ti-0.5%	7590	0.01	0.05	0.03	0.05	5
Cr-Ti-1%	14,269	0.02	0.03	0.06	0.08	5
Cr-Ti-2%	27,904	0.04	0.05	0.11	0.06	5
Cr-Fe-0%	0	0.00	0.01	0.01	0.02	5
Cr-Fe-0.01%	205	0.00	0.01	-0.08	0.04	5
Cr-Fe-S14	558	0.02	0.02	0.01	0.02	[1]
Cr-Fe-0.1%	2505	0.01	0.01	-0.04	0.05	5
Cr-Fe-0.5%	11,846	-0.01	0.02	-0.19	0.04	5
Cr-Na-50%		0.04	0.05	0.11	0.05	4
Cr-Na-100%		0.01	0.02	0.02	0.09	4
Cr-K-50%		0.03	0.05	0.04	0.02	4
Cr-K-100%		0.01	0.02	0.01	0.10	4
Allende-1		0.08	0.01	0.87	0.08	5
Allende-2		0.10	0.02	0.90	0.02	5
Allende-3		0.11	0.02	0.94	0.02	5
Allende-4		0.14	0.03	0.95	0.08	5
Allende-5		0.10	0.02	0.96	0.05	5
Average		0.10	0.04	0.92	0.07	2SD
DTS-1-1		0.05	0.01	0.11	0.07	5
DTS-1-2		0.05	0.01	0.16	0.05	5
DTS-1-3		0.06	0.03	0.18	0.07	5
DTS-1-4		0.04	0.03	0.15	0.03	5
DTS-1-5		0.07	0.02	0.19	0.07	5
Average		0.05	0.03	0.16	0.06	2SD
Orgueil-1		0.19	0.05	1.51	0.05	5
Orgueil-2		0.19	0.01	1.50	0.08	5
Average		0.19	0.00	1.50	0.01	2SD

Note: The references [1] Schiller et al. (2014). The doped samples are the corresponding SCP elemental standards of ICP-MS.

* The corresponding V, Ti and Fe interference is for ^{50}Cr , ^{50}Cr and ^{54}Cr respectively.

Table 3
Comparison of $^{55}\text{Mn}/^{52}\text{Cr}$ and Cr isotope data for meteorites that have been measured multiple times here and/or in the literature.

	Mass (mg)	$^{55}\text{Mn}/^{52}\text{Cr}$	$\epsilon^{53}\text{Cr}$	Error	$\epsilon^{54}\text{Cr}$	Error	N	Instruments	Ref.
Orgueil		0.87	0.43	0.10			11	Nu Plasma HR MC-ICP-MS	(Moynier et al. 2007)
Orgueil	992	0.81	0.39	0.10	1.51	0.20	110	VG-54E and Micromass Sector 54 TIMS	(Shukolyukov and Lugmair, 2006)
Orgueil	39.0	0.93	0.46	0.06	1.94	0.12	n.d.	Triton TIMS	(Kadlag et al., 2019)
Orgueil	22.6	0.86	0.19	0.05	1.51	0.05	5	Neptune Plus MC-ICP-MS	This study
Orgueil	22.6		0.19	0.01	1.50	0.08	5	Neptune Plus MC-ICP-MS	This study
Orgueil	46	0.80	0.25	0.06	1.56	0.06	3-5	Triton TIMS	(Trinquier et al., 2007, 2008a, 2008b)
Orgueil	~100	0.85	0.20	0.05	1.55	0.13	6-10	Triton TIMS	(Qin et al., 2010)
Orgueil			0.24	0.05	1.69	0.09	6-10	Triton TIMS	(Qin et al., 2010)
Orgueil	320	0.81	0.25	0.03	1.56	0.06	n.d.	Triton TIMS	(Petit et al., 2011)
Averaged value		0.85	0.29	0.07	1.60	0.10			
Ivuna	225	0.82	0.41	0.11	1.59	0.24	71	VG-54E and Micromass Sector 54 TIMS	(Shukolyukov and Lugmair, 2006)
Ivuna	30.5	0.94	0.30	0.17	1.79	0.20	n.d.	Triton TIMS	(Kadlag et al., 2019)
Ivuna		0.75	0.16	0.02	1.55	0.05	10	Neptune Plus MC-ICP-MS	(Schiller et al., 2014)
Ivuna	~200	0.85	0.25	0.06	1.59	0.14	12	Triton TIMS (Total Evaporation)	This study; (van Kooten et al., 2016)
					1.30	0.09		Triton Plus TIMS	(Williams et al., 2020)
Averaged value		0.84	0.28	0.10	1.56	0.15			
Allende	~100	0.42	0.08	0.01	0.87	0.08	5	Neptune Plus MC-ICP-MS	This study
Allende	~100		0.10	0.02	0.90	0.02	5	Neptune Plus MC-ICP-MS	This study
Allende	~100		0.11	0.02	0.94	0.02	5	Neptune Plus MC-ICP-MS	This study
Allende	~100		0.14	0.03	0.95	0.08	5	Neptune Plus MC-ICP-MS	This study
Allende	~100		0.10	0.02	0.96	0.05	5	Neptune Plus MC-ICP-MS	This study
Allende	~50	0.42	0.10	0.06	1.10	0.08	8	Neptune Plus MC-ICP-MS	(Zhu et al., 2020b)
Allende		0.42	0.16	0.06	0.88	0.17	15	Triton TIMS (Total Evaporation)	(Zhu et al., 2020a)

	Mass (mg)	$^{55}\text{Mn}/^{52}\text{Cr}$	$\epsilon^{53}\text{Cr}$	Error	$\epsilon^{54}\text{Cr}$	Error	N	Instruments	Ref.
Allende	81	0.45	0.04	0.06	0.86	0.09	3-5	Triton TIMS	(Trinquier et al., 2007, 2008a, 2008b)
Allende	~100		0.14	0.04	0.98	0.14	6-10	Triton TIMS	(Qin et al., 2010)
Allende	~100		0.13	0.05	0.92	0.13	6-10	Triton TIMS	(Qin et al., 2010)
Allende		0.43	0.14	0.11			5	Nu Plasma HR MC-ICP-MS	(Moynier et al., 2007)
Allende	2380	0.43	0.10	0.09	0.85	0.17	70	VG-54E and Micromass Sector 54 TIMS	(Shukolyukov and Lugmair, 2006)
Allende	44.3	0.51	0.07	0.08	1.24	0.24	n.d.	Triton TIMS	(Kadlag et al., 2019)
Allende					0.86	0.09	4	Triton Plus TIMS	(Williams et al., 2020)
Averaged value		0.44	0.11	0.02	0.95	0.06			
Vigarano	21.0	0.42	0.08	0.02	0.84	0.04	5	Neptune Plus MC-ICP-MS	This study
Vigarano	~100	0.57	0.22	0.07	0.91	0.12	6-10	Triton TIMS	(Qin et al., 2010)
Vigarano	~100		0.14	0.05	0.82	0.13	6-10	Triton TIMS	(Qin et al., 2010)
Vigarano			0.23	0.08			12	Nu Plasma HR MC-ICP-MS	(Moynier et al., 2007)
Averaged value		0.49	0.17	0.07	0.86	0.05			
Leoville	24.8	0.41	0.08	0.04	0.81	0.10	5	Neptune Plus MC-ICP-MS	This study
Leoville	~100	0.46	0.12	0.04	0.71	0.15	6-10	Triton TIMS	(Qin et al., 2010)
Averaged value		0.43	0.10	0.04	0.76	0.10			
Renazzo	12	0.54	0.20	0.10	1.30	0.21	3-5	Triton TIMS	(Trinquier et al., 2007, 2008a, 2008b)
Renazzo					1.22	0.10	4	Triton Plus TIMS	(Sanborn et al., 2019)
Averaged value	0.54	0.20	0.10	1.26	0.08				
Jbilet Winselwan	19.5	0.56	0.12	0.02	0.82	0.04	5	Neptune Plus MC-ICP-MS	This study
Jbilet Winselwan	~150	0.63	0.19	0.06	1.01	0.12	16	Triton TIMS (Total Evaporation)	(van Kooten et al. 2020)
Averaged value		0.59	0.16	0.07	0.92	0.18			
Murchison		0.64	0.27	0.06	1.01	0.05	3-5	Triton TIMS	(Trinquier et al., 2007, 2008a, 2008b)
Murchison	~150	0.67	0.19	0.04	0.93	0.07	16	Triton TIMS (Total Evaporation)	(van Kooten et al. 2020)
Murchison	~100	0.60	0.17	0.08	0.97	0.20	6-10	Triton TIMS	(Qin et al., 2010)
Murchison			0.16	0.04	0.89	0.08	4	Triton Plus TIMS	(Jenniskens et al., 2012)
Averaged value		0.64	0.20	0.05	0.95	0.05			
Murray	101	0.64	0.27	0.09	1.13	0.21	93	VG-54E and Micromass	(Shukolyukov and Lugmair, 2006)

	Mass (mg)	$^{55}\text{Mn}/^{52}\text{Cr}$	$\epsilon^{53}\text{Cr}$	Error	$\epsilon^{54}\text{Cr}$	Error	N	Instruments	Ref.
								Sector 54 TIMS	
Murray	~150	0.63	0.18	0.03	0.85	0.10	16	Triton TIMS (Total Evaporation)	(van Kooten et al. 2020)
Averaged value		0.63	0.23	0.09	0.99	0.27			
Kainsaz	1030	0.54	0.20	0.10	1.02	0.24	91	VG-54E and Micromass Sector 54 TIMS	(Shukolyukov and Lugmair, 2006)
Kainsaz	~100	0.52	0.13	0.06	0.87	0.18	6-10	Triton TIMS	(Qin et al., 2010)
Averaged value		0.53	0.17	0.07	0.95	0.15			
Lance'	8	0.47	-0.04	0.07	0.57	0.11	3-5	Triton TIMS	(Trinquier et al., 2007, 2008a, 2008b)
Lance'		0.50	0.20	0.09			15	Nu Plasma HR MC-ICP-MS	(Moynier et al. 2007)
Karoonda	33.9	0.41	0.04	0.02	0.50	0.09	5	Neptune Plus MC-ICP-MS	This study
Karoonda	25	0.48	0.14	0.06	0.63	0.09	3-5	Triton TIMS	(Trinquier et al., 2007, 2008a, 2008b)
Averaged value		0.44	0.09	0.10	0.57	0.13			
EET 92002	34.6	0.41	0.10	0.04	0.52	0.09	5	Neptune Plus MC-ICP-MS	This study
EET 92002	~100	0.46	0.02	0.05	0.33	0.12	6-10	Triton TIMS	(Qin et al., 2010)
Averaged value		0.43	0.06	0.08	0.43	0.19			
Qingzhen			0.12	0.04	0.00	0.05	5	Triton TIMS	(Mougel et al., 2018)
Qingzhen	260	0.72	0.20	0.06			3-5	Triton TIMS	(Trinquier et al., 2007, 2008a, 2008b)
Qingzhen	260	0.72	0.17	0.06	-0.02	0.08	3-5	Triton TIMS	(Trinquier et al., 2007, 2008a, 2008b)
Average value		0.72	0.16	0.05	-0.01	0.02		Triton TIMS	(Trinquier et al., 2007, 2008a, 2008b)
Kota-Kota		n.d.	0.11	0.04	0.00	0.08	6	Triton TIMS	(Mougel et al., 2018)
Kota-Kota		0.69	0.18	0.06	-0.02	0.21	3-5	Triton TIMS	(Trinquier et al., 2007, 2008a, 2008b)
Kota-Kota		0.69	0.17	0.06	0.04	0.07	3-5	Triton TIMS	(Trinquier et al., 2007, 2008a, 2008b)
Averaged value		0.69	0.15	0.04	0.01	0.03			
Abee			0.05	0.04	-0.02	0.08	4	Triton TIMS	(Mougel et al., 2018)
Abee	18	0.93	0.26	0.08	-0.06	0.12	3-5	Triton TIMS	(Trinquier et al., 2007, 2008a, 2008b)
Averaged value		0.93	0.16	0.21	-0.04	0.04			

	Mass (mg)	$^{55}\text{Mn}/^{52}\text{Cr}$	$\epsilon^{53}\text{Cr}$	Error	$\epsilon^{54}\text{Cr}$	Error	N	Instruments	Ref.
SAH 97096	33.2	0.65	0.25	0.03	0.17	0.08	5	Neptune Plus MC-ICP-MS	This study
SAH 97096		0.65	0.19	0.04	-0.01	0.14	14	Triton TIMS (Total Evaporation)	(Zhu et al., 2020a)
Averaged value		0.65	0.22	0.06	0.08	0.18			
MIL 05082	96.4*	0.37	0.20	0.01	1.50	0.09	5	Neptune Plus MC-ICP-MS	This study
QC 001	39.8	0.47	0.19	0.04	1.45	0.06	5	Neptune Plus MC-ICP-MS	This study
HaH 237	32.9	0.09	0.05	0.03	1.42	0.04	5	Neptune Plus MC-ICP-MS	This study
HaH 237	679	0.08	-0.15	0.09	0.87	0.19	148	VG-54E and Micromass Sector 54 TIMS	(Shukolyukov and Lugmair, 2006)
Bencubbin (silicate<metal)		0.04	-0.05	0.06	1.11	0.09	3-5	Triton TIMS	(Trinquier et al., 2007, 2008a, 2008b)
Bencubbin(metal<silicate)		0.48	0.12	0.09	1.13	0.09	3-5	Triton TIMS	(Trinquier et al., 2007, 2008a, 2008b)
Gujba metal chondrule		0.20	-0.03	0.13	1.07	0.27	3-5	Triton TIMS	(Trinquier et al., 2007, 2008a, 2008b)

Note: The error for Mn/Cr ratios is 5%. The mass marked* means a chip. The uncertainty of average values are 95% confidence intervals.

Table 4
The Mn/Cr ratio, and Cr and O isotope data for all chondrites.

Carbonaceous Chondrites	Fall/Find	Mass (mg)	Type	$^{55}\text{Mn}/^{52}\text{Cr}$	$\epsilon^{53}\text{Cr}$	Error	$\epsilon^{54}\text{Cr}$	Error	N/[ref.]	^{17}O	Error	[ref.]
Orgueil	fall	22.6	CI1	0.85	0.29	0.07	1.60	0.10	[This study, 2, 4, 5, 21, 30, 31, 32]	0.39	0.08	[9]
Ivuna	fall	CI1	0.84	0.28	0.10	1.56	0.15	[1, 22, 29, 30, 32]	0.47	0.08	[9]	
CI average				0.84	0.28	0.01	1.56	0.05	2SD			
PCA 91467*	find	28.5	CH3	0.36	0.13	0.00*	1.50	0.08	5	-1.47	0.08	[9]
A-881020*	find	40.5	CH3	0.33	0.11	0.03	1.49	0.06	5			
CH average				0.34	0.12	0.03	1.50	0.01	2SD			
MIL 05082*	find	96.4	CB3	0.37	0.20	0.01	1.50	0.09	5			
QC 001*	find	39.8	CBa3	0.47	0.19	0.04	1.45	0.06	5			
Bencubbin*	find		CBa3				1.12	0.03	[2]	-1.75	0.08	[9]
Gujba*	fall		CBa3				1.29	0.07	[3]	-2.38	0.08	[10]
HaH 237*	find	32.9	CBb3	0.09	0.05	0.03	1.42	0.04	5	-0.77	0.08	[11]
CB average				0.42	0.20	0.01	1.36	0.30	2SD			
GRO 95577	find	20.5	CR1	0.51	0.15	0.02	1.25	0.06	5	-0.45	0.08	[9]
Al Rais	fall	23.2	CR2-an	0.60	0.19	0.01	1.24	0.11	5	-1.01	0.08	[9]
Renazzo	fall		CR2	0.54	0.20	0.10	1.26	0.08	[2, 4, 24]	-0.96	0.08	[9]
GRA 06100	find		CR2	0.58	0.25	0.05	1.32	0.11	[5]	-1.80	0.03	[20]
NWA 6043	find		CR2	0.58	0.07	0.07	1.24	0.10	[22, 23]			
EET 92161	find		CR2	0.50	0.21	0.04	1.19	0.12	[22, 23]			
NWA 7837	find		CR2	0.39	0.02	0.04	1.06	0.08	[22, 23]			
GRA 95229	find		CR2				1.18	0.07	[29]	-2.19	0.01	[29]
QUE 99177	find		CR2				1.43	0.12	[29]	-2.89	0.12	[29]
LAP 02342	find		CR2				1.49	0.11	[29]	-2.45	0.06	[29]
NWA 6921	find		CR6				1.32	0.09	[24,29]	-1.74	0.01	[29]
NWA 7317	find		CR6				1.32	0.09	[24]			
CR average				0.53	0.16	0.16	1.28	0.23	2SD			
SCO 06043	find	21.7	CM1	0.60	0.22	0.02	1.13	0.12	5			
Nogoya	fall	24.3	CM2	0.59	0.18	0.05	0.76	0.04	5	-2.00	0.08	[9]
Banten	fall	21.7	CM2	0.58	0.12	0.03	0.86	0.05	5	-2.97	0.08	[9]
Aguas Zarcas	fall	87.7	CM2	0.60	0.15	0.03	0.86	0.03	5	-2.78	0.20	[18]
Jbilet Winselwan	find	19.5	CM2	0.59	0.16	0.10	0.92	0.18	[This study, 23]	-4.03	0.55	[18]
Paris	find		CM2	0.62	0.16	0.05	0.93	0.09	[6]	-3.39	0.39	[19]
NWA 8157	find		CM2	0.62	0.20	0.11	1.01	0.18	[6]	-4.05	0.55	[18]
Murchison	fall		CM2	0.64	0.20	0.11	0.95	0.04	[2, 4, 5, 23, 28]	-2.60	0.08	[12]

Carbonaceous Chondrites	Fall/Find	Mass (mg)	Type	$^{55}\text{Mn}/^{52}\text{Cr}$	$\epsilon^{53}\text{Cr}$	Error	$\epsilon^{54}\text{Cr}$	Error	N/[ref.]	^{17}O	Error	[ref.]
Mighei	fall		CM2	0.63	0.18	0.03	0.74	0.10	[23]	-2.50	0.08	[9]
Cold Bokkeveld	fall		CM2	0.65	0.07	0.03	0.81	0.12	[23]	-2.45	0.08	[9]
Murray	fall		CM2	0.63	0.23	0.09	0.99	0.27	[23, 30]	-3.07	0.08	[9]
Maribo	fall		CM2	0.65	0.29	0.04	1.13	0.15	[23]			
Diepenveen	fall		CM2-an		0.13	0.05	0.85	0.10	[27]			
CM average				0.62	0.17	0.11	0.92	0.26	2SD			
Allende	fall	~100	CV3-oxA	0.44	0.11	0.02	0.95	0.06	[This study, 2, 4, 5, 25, 26, 28, 30, 31, 32]	-3.62	0.06	[13]
Bali	fall	42.3	CV3-oxB	0.45	0.13	0.04	1.10	0.06	5	-3.30	0.17	[13]
Mokoia	fall	20.5	CV3-oxB	0.45	0.11	0.04	1.00	0.01	5	-3.18	0.07	[13]
Leoville	find	24.8	CV3-red	0.43	0.10	0.04	0.76	0.10	[This study, 5]	-4.69	0.17	[13]
Vigarano	fall	21.0	CV3-red	0.49	0.13	0.10	0.85	0.02	[This study, 5, 31]	-4.25	0.03	[13]
Kaba	fall	19.7	CV3-oxB	0.43	0.08	0.05	0.70	0.07	5	-3.43	0.31	[13]
CV average				0.45	0.11	0.04	0.89	0.30	2SD			
MIL 07193	find	20.9	CO3	0.48	0.16	0.02	1.22	0.04	5			
DOM 10104	find	24.7	CO3	0.48	0.09	0.03	0.80	0.06	5			
Ormans	fall	66.2	CO3	0.50	0.12	0.01	0.90	0.03	5	-4.45	0.08	[9]
Felix	fall		CO3	0.47	0.07	0.06	0.63	0.09	[2, 4]	-4.59	0.08	[9]
Kainsaz	fall		CO3	0.53	0.17	0.07	0.95	0.15	[5, 31]	-4.72	0.08	[9]
CO average				0.49	0.11	0.07	0.90	0.43	2SD			
ALH 85002	find	45.8	CK4	0.42	0.06	0.02	0.46	0.05	5			
Karoonda	fall	33.9	CK4	0.44	0.09	0.10	0.57	0.13	[This study, 2, 4]	-4.55	0.00	[13]
EET 92002	find	34.6	CK5	0.43	0.06	0.08	0.43	0.19	[This study, 5]			
LEW 87009	find	43.8	CK6	0.44	0.08	0.04	0.58	0.05	5	-4.32	0.08	[9]
CK average				0.43	0.07	0.03	0.51	0.15	2SD			
Ordinary Chondrites												
Roosevelt	find		H3.4	0.65	0.17	0.02	-0.44	0.03	[7]			
Brownstried	find		H3.7	0.67	0.18	0.02	-0.44	0.03	[7]			
Ochansk	fall		H4	0.64	0.15	0.02	-0.40	0.03	[7]	0.82	0.08	[14]
LAP 03601	find		H4	0.78	0.21	0.06	-0.28	0.11	[5]			
Ste. Marguerite	fall		H4	0.63	0.13	0.06	-0.39	0.07	[2, 4]			
Beaver Creek	fall		H4	0.70	0.17	0.02	-0.40	0.04	[7]	0.76	0.08	[14]
Bath	fall		H4	0.68	0.17	0.02	-0.36	0.04	[7]	0.71	0.08	[14]
Menow	fall		H4	0.66	0.12	0.02	-0.43	0.03	[7]			
Forest city	fall		H5	0.71	0.18	0.02	-0.36	0.03	[7]	0.75	0.08	[14]

Carbonaceous Chondrites	Fall/Find	Mass (mg)	Type	$^{55}\text{Mn}/^{52}\text{Cr}$	$\epsilon^{53}\text{Cr}$	Error	$\epsilon^{54}\text{Cr}$	Error	N/[ref.]	^{17}O	Error	[ref.]
Estacado	find		H6	0.67	0.15	0.02	-0.35	0.06	[7]			
Aarhus	fall		H6	0.68	0.17	0.01	-0.41	0.03	[7]			
Kernouve	fall		H6	0.72	0.19	0.06	-0.37	0.07	[2, 4]			
Portales Valley	fall		H6/7	0.74	0.19	0.02	-0.37	0.04	[7]			
H average				0.69	0.17	0.05	-0.38	0.09	2SD			
QUE 97008	find		L3	0.72	0.17	0.06	-0.42	0.14	[5]			
Bjurböle	fall		L4	0.81	0.20	0.06			[4]	1.00	0.08	[14]
Knyahinya	fall		L5	0.70	0.15	0.06	-0.38	0.08	[2, 4]	1.05	0.08	[14]
Holbrook	fall		L6	0.80	0.23	0.06			[4]			
L average				0.76	0.19	0.07	-0.40	0.06	2SD			
Chainpur	fall		LL3-4	0.85	0.24	0.06	-0.47	0.07	[2, 4]			
Soko-Banja	fall		LL4	0.82	0.34	0.06			[4]	1.32	0.08	[14]
GRO 95552	find		LL4	0.78	0.19	0.04	-0.33	0.10	[5]			
Olivenza	fall		LL5	0.76	0.23	0.06			[4]	1.11	0.08	[14]
Guider	fall		LL5	0.99	0.21	0.06			[4]	1.19	0.08	[14]
Saint-Se'verin	fall		LL6	0.77	0.28	0.06	-0.41	0.10	[2, 4]	1.16	0.08	[14]
LL average				0.83	0.25	0.04	-0.40	0.14	2SD			
OC average				0.74	0.19	0.10	-0.39	0.09	2SD			
Enstatite Chondrites												
SAH 97096	find	33.2	EH3	0.65	0.22	0.06	0.08	0.18	[This study, 26]	-0.07	0.02	[17]
Qingzhen	fall		EH3	0.72	0.15	0.07	-0.01	0.02	[2,4,8]	-0.03	0.08	[15]
Kota-Kota	find		EH3	0.69	0.14	0.07	0.01	0.01	[2,4,8]	-0.15	0.08	[15]
ALHA 77295	find		EH3	0.71	0.14	0.06	0.05	0.14	[5]			
Abee	fall		EH4	0.93	0.16	0.21	-0.04	0.04	[2,4,8]	0.19	0.19	[17]
Indarch	fall		EH4	0.91	0.21	0.07	0.05	0.14	[5]	0.12	0.08	[15]
EH average				0.77	0.17	0.07	0.02	0.09	2SD			
MAC 88136	find		EL3	0.72	0.15	0.03	0.02	0.09	[5]	-0.11	0.04	[17]
MAC 88184	find		EL3	0.20	0.03	0.11	0.07	[8]				
Hvittis	fall		EL6	0.67	0.14	0.07	-0.01	0.17	[2,4]	0.07	0.08	[15]
Pillistfer	fall		EL6	0.59	0.15	0.05	0.09	0.08	[2,4]	0.02	0.08	[15]
LON 94100	find		EL6	0.56	0.17	0.04	-0.02	0.14	[5]			
Eagle	fall		EL6	0.14	0.05	-0.07	0.07	[8]				
EL average				0.63	0.16	0.05	0.02	0.14	2SD			
EC average				0.71	0.16	0.06	0.02	0.11	2SD			

Note: The references: [1] Schiller et al. (2014), [2] Trinquier et al. (2007), [3] Yamashita et al. (2010), [4] Trinquier et al. (2008a), [5] Qin et al. (2010), [6] Göpel et al. (2015), [7] Pedersen et al. (2019), [8] Mougél et al. (2018), [9] Clayton and Mayeda (1999), [10] Rubin et al. (2001), [11] Weisberg et al. (2001), [12] Clayton and Mayeda (1984), [13] Greenwood et al. (2010), [14] Clayton et al. (1991), [15] Clayton et al. (1984), [16] Greenwood et al. (2017), [17] Newton et al. (2000), [18] Meteoritical Bulletin, [19] Hewins et al. (2014), [20] Schrader et al. (2011), [21] Petit et al. (2011), [22] Van Kooten et al. (2016), [23] van Kooten et al. (2020), [24] Sanborn et al. (2019), [25] Zhu et al. (2020b), [26] Zhu et al. (2020a), [27] Langbroek et al. (2019), [28] Jenniskens et al. (2012), [29] Williams et al. (2020), [30] Shukolyukov and Lugmair (2006), [31] Moynier et al. (2007) and [32] Kadlag et al. (2019).

The errors for $^{55}\text{Mn}/^{52}\text{Cr}$ ratios are 5%. The $^{55}\text{Mn}/^{52}\text{Cr}$ for H chondrite samples in [7] Pedersen et al. (2019) are re-measured (same solution) by MC-ICP-MS in this study.

The Fe/Cr (atom) ratios for CB and CH chondrites: PCA 91467, 97; A-881020, 115; QC 001, 25; HaH 237, 235

The errors for O isotope data in [18] are 1SD of multiple O isotope data, and in [10] and [11] are quoted as 0.08 from [9].

* The $\epsilon^{53}\text{Cr}$ 2SE uncertainty for PCA 91467 is less than 0.004. The CB and CH samples in this study, including PCA 91467, MIL 05082, A-881020, QC 001 and HaH 237 may not represent the bulk composition of the parent chondrites given the clear evidence for sample heterogeneity in CB and CH chondrites and the fact that the mass of our samples is relatively small. The $\epsilon^{54}\text{Cr}$ data for Bencubbin is the average (with 2SD uncertainty) of two data (silicate > metal and silicate < metal) in Trinquier et al. (2007). The $\epsilon^{54}\text{Cr}$ data for Gujba is the average (with 2SD uncertainty) of the data for chondrules and metals in Yamashita et al. (2010).

Table 5
The Cr and O isotope compositions of various Solar System materials not analyzed here
(including: Rumuruti chondrites, terrestrial planets and achondrite parent bodies).

Meteorites/Planets	$\epsilon^{54}\text{Cr}$	Error (2SD)	N	Ref.	^{17}O	error	N	Ref.
Rumuruti (R) chondrites	-0.06	0.08	12	[35]	2.72	0.31	24	[36]
Earth	0.09	0.12	15	[2, 8, 25, this study]	-0.01	0.01	14	[26]
Moon	0.09	0.08	/	[8]	-0.01	0.02	22	[26]
Aubrites	-0.16	0.19	1	[2]	-0.01	0.11	13	[26]
Mars (SNC meteorites)	-0.17	0.15	18	[2, 33]	0.28	0.08		[34]
Angrite parent body (APB)	-0.42	0.13	8	[2, 22]	-0.07	0.01	5	[26]
Brachinites	-0.44	0.23	2	[29]	-0.17	0.09	2	[29]
Winonaites	-0.53	0.02	3	[23]	-0.51	0.08	16	[26]
Acapulcoite-Iodranite Clan	-0.61	0.19	6	[23]	-1.12	0.36	23	[26]
Vesta (HED meteorites)	-0.73	0.08	9	[2]	-0.24	0.02	105	[26]
Ureilite parent body (UPB)	-0.95	0.15	18	[24, 25]	-0.96	1.00	42	[26]

Note: The reference sources are: [2] Trinquier et al. (2007), [8] Mougél et al. (2018), [22] Zhu et al. (2019b), [23] Li et al. (2018), [24] Zhu et al. (2020b), [25] Yamakawa et al. (2010), [26] Greenwood et al. (2017), [25] Zhu et al. (2020b), [29] Williams et al. (2020), [33] Kruijer et al. (2020), [34] Ireland et al. (2020), [35] Zhu et al. (2021) and [36] Bischoff et al. (2011). The $\epsilon^{54}\text{Cr}$ values are calculated by mean average. The O isotope data did not consider Cumberland falls for aubrites and some isotopically anomalous eucrites for Vesta. The N (/) of $\epsilon^{54}\text{Cr}$ value of Moon means it was modeled by the correlation of the $\epsilon^{53}\text{Cr}$ and $\epsilon^{54}\text{Cr}$ of lunar samples that had been influenced by cosmogenic effects. The $\epsilon^{54}\text{Cr}$ for Nakhla (Mars) is chosen from [2], due to the smaller uncertainty.

Table 6
Cr isotope data for artificial standards and terrestrial samples.

Sample Name	Petrology	$\epsilon^{53}\text{Cr}$	2se	$\epsilon^{54}\text{Cr}$	2se	N/[ref.]
NIST 3112a	Artificial standard	0.04	0.03	0.03	0.05	5
SCP-Cr	Artificial standard	0.02	0.02	0.05	0.08	5
DTS-1	Dunite	0.05	0.03	0.16	0.06	5, 2SD
DTS-2b	Dunite	0.04	0.01	0.08	0.06	[1]
PCC-1	Peridotite	0.05	0.03	0.10	0.07	[25]
KOLA15-UB	Peridotite	0.00	0.03	0.05	0.06	[8]
BM31	Peridotite	0.07	0.04	0.13	0.08	[8]
BM23	Peridotite	-0.01	0.05	0.03	0.08	[8]
Tibet chromite	Chromite	0.03	0.07	0.08	0.08	[2, 4]
Deccan basalt	Basalt	0.03	0.08	0.08	0.15	[2, 4]
Erta Ale tholeite	Basalt	-0.02	0.06	-0.02	0.08	[2, 4]
10PUB22-07	Basalt	0.08	0.05	0.19	0.07	[8]
KBD408729	Basalt	0.07	0.03	0.14	0.07	[8]
NIST 688	Basalt	0.06	0.04	0.11	0.07	[8]
CV-SN-98-19	Basalt	0.01	0.05	0.12	0.11	[8]
BE-N	Basalt	0.12	0.03	0.17	0.07	[8]
BHVO-2	Basalt	0.02	0.03	0.07	0.07	[8]
Average		0.04	0.02	0.09	0.03	2SE, N = 15
			0.08		0.12	2SD, N = 15

Note: The average data for terrestrial samples (N = 15) do not include the two artificial standards. The reference sources are [1] Schiller et al. (2014), [2] Trinquier et al. (2007), [4] Trinquier et al. (2008a), [8] Mougél et al. (2018) and [25] Zhu et al. (2020b).

Table 7a
Parameters for theoretical calculation for Cr isotope fractionation.

	Mass of isotopes	Isotope abundance	CrO	CrO ₂	CrO ₃
⁵⁰ Cr	49.946	4.345%	65.941	81.936	97.931
⁵² Cr	51.941	83.789%	67.935	83.930	99.925
⁵³ Cr	52.941	9.501%	68.936	84.930	100.925
⁵⁴ Cr	53.939	2.365%	69.934	85.929	101.924
¹⁶ O	15.995				

Table 7b
The calculated Cr isotope data based on different Cr oxides and different laws (kinetic and equilibrium), assuming the initial $^{50}\text{Cr}/^{52}\text{Cr}$ fractionation is 1000ppm.

	50/52	53/52	54/52	$\beta^{53}\text{Cr}$	$\beta^{54}\text{Cr}$	^{53}Cr	^{54}Cr	54/53 factors
Kin. Cr	1000	-487.09	-964.17	-2.05	-1.04	0.00	0.00	
Kin. CrO	1000	-490.46	-972.94	-2.04	-1.03	-3.37	-8.77	2.606
Kin. CrO ₂	1000	-492.55	-978.41	-2.03	-1.02	-5.45	-14.24	2.611
Kin. CrO ₃	1000	-493.97	-982.14	-2.02	-1.02	-6.88	-17.97	2.614
Equ. Cr	1000	-473.09	-927.79	-2.11	-1.08	14.00	36.38	2.598
Equ. CrO	1000	-479.68	-944.75	-2.08	-1.06	7.42	19.41	2.617
Equ. CrO ₂	1000	-483.78	-955.40	-2.07	-1.05	3.32	8.76	2.643
Equ. CrO ₃	1000	-486.58	-962.71	-2.06	-1.04	0.51	1.46	2.838

Note: The fractionation factors, $\beta^{53}\text{Cr}$ and $\beta^{54}\text{Cr}$, are calculated by Eqs. (9) and (12) in Young and Galy (2004).